MIT Libraries | DSpace@MIT

MIT Open Access Articles

S-nitrosation of proteins relevant to Alzheimer's disease during early stages of neurodegeneration

Massachusetts Institute of Technology

S-nitrosation of proteins relevant to Alzheimer's disease during early stages of neurodegeneration

Uthpala Seneviratne[a,1], Alexi Nott[b,1], Vadiraja B. Bhat[c], Kodihalli C. Ravindra[a], John S. Wishnok[a], Li-Huei Tsai[b], and Steven R. Tannenbaum[a,d,2]

[a]Department of Biological Engineering, Massachusetts Institute of Technology, Cambridge, MA 02139; [b]The Picower Institute for Learning and Memory, Department of Brain and Cognitive Sciences, Massachusetts Institute of Technology, Cambridge, MA 02139; [c]Agilent Technologies, Inc., Wilmington, DE 19808; and [d]Department of Chemistry, Massachusetts Institute of Technology, Cambridge, MA 02139

Protein S-nitrosation (SNO-protein), the nitric oxide-mediated posttranslational modification of cysteine thiols, is an important regulatory mechanism of protein function in both physiological and pathological pathways. A key first step toward elucidating the mechanism by which S-nitrosation modulates a protein's function is identification of the targeted cysteine residues. Here, we present a strategy for the simultaneous identification of SNO-cysteine sites and their cognate proteins to profile the brain of the CK-p25–inducible mouse model of Alzheimer's disease-like neurodegeneration. The approach—SNOTRAP (SNO trapping by triaryl phosphine)—is a direct tagging strategy that uses phosphine-based chemical probes, allowing enrichment of SNO-peptides and their identification by liquid chromatography tandem mass spectrometry. SNOTRAP identified 313 endogenous SNO-sites in 251 proteins in the mouse brain, of which 135 SNO-proteins were detected only during neurodegeneration. S-nitrosation in the brain shows regional differences and becomes elevated during early stages of neurodegeneration in the CK-p25 mouse. The SNO-proteome during early neurodegeneration identified increased S-nitrosation of proteins important for synapse function, metabolism, and Alzheimer's disease pathology. In the latter case, proteins related to amyloid precursor protein processing and secretion are S-nitrosated, correlating with increased amyloid formation. Sequence analysis of SNO-cysteine sites identified potential linear motifs that are altered under pathological conditions. Collectively, SNOTRAP is a direct tagging tool for global elucidation of the SNO-proteome, providing functional insights of endogenous SNO proteins in the brain and its dysregulation during neurodegeneration.

S-nitrosation | Alzheimer's disease | secretase pathway | presenilin pathway | neurodegeneration

Protein S-nitrosation (SNO-protein), in which a cysteine (Cys) thiol is converted to a nitrosothiol (RSNO), is an important posttranslational modification (PTM). Cys residues targeted for S-nitrosation often impact enzyme activity, protein localization, and protein–protein interactions (1). SNO begins with the production of nitric oxide radicals (NO$^\bullet$) via conversion of L-arginine to L-citrulline by nitric oxide synthase 1 (NOS1) (neuronal), NOS2 (inducible), and NOS3 (endothelial). NO-mediated SNO PTMs are thought to occur in vivo predominantly through radical recombination between NO$^\bullet$ and a thiyl radical, transnitrosation by low-molecular weight NO carriers such as S-nitrosoglutathione (GSNO), or protein-assisted transnitrosation (2–8). In the healthy brain, low levels of NO and normal SNO PTMs play important roles in regulating synaptic plasticity, gene expression, and neuronal survival. In contrast, elevated NO levels associated with aging and environmental stress have been linked to neurological pathologies, including Alzheimer's (AD), Parkinson's, and Huntington's disease (9). AD is the most prevalent form of human dementia, with a frequency that progressively increases in aging societies (10). A pivotal role in development and progression of late-onset AD, and other age-dependent dementias, has been attributed to inflammatory and oxidative stress cascades in the brain (11, 12), which are potentiated by elevated levels of nitrosating and oxidizing species (13, 14).

Despite the biological importance of this PTM, significant gaps exist regarding its in vivo specificity and origin. Characterization of endogenous proteins suggests that not all reduced Cys residues on a given protein and not all Cys-containing proteins are S-nitrosated, implying a biased selection. Although S-nitrosation has been frequently reported, the specific SNO residues for many of the proteins have not been determined and can be critical for determining their function. Currently, the identification of a specific SNO residue involves an iterative combination of mutagenic and mass spectrometry (MS)-based approaches. The prototypical method for detecting SNO-proteins is the biotin-switch technique (BST), which requires blocking of all free Cys-thiols, followed by selective ascorbate reduction of SNO-Cys residues that are biotinylated and isolated for analysis (9, 15–17). One limitation of the BST is that false positives can occur through incomplete blocking of free Cys-thiols, making them difficult to distinguish from true SNO-Cys residues. The variability of the BST and similar methods has driven a search for

Significance

Protein S-nitrosation (SNO-protein) is a posttranslational modification in which a cysteine (Cys) residue is modified by nitric oxide (SNO-Cys). SNO-proteins impact many biological systems, but their identification has been technically challenging. We developed a chemical proteomic strategy—SNOTRAP (SNO trapping by triaryl phosphine)—that allows improved identification of SNO-proteins by mass spectrometry. We found that S-nitrosation is elevated during early stages of neurodegeneration, preceding cognitive decline. We identified changes in the SNO-proteome during early neurodegeneration that are potentially relevant for synapse function, metabolism, and Alzheimer's disease pathology. SNO-proteome analysis further reveals a potential linear motif for SNO-Cys sites that are altered during neurodegeneration. Our strategy can be applied to multiple cellular and disease contexts and can reveal signaling networks that aid drug development.

alternative approaches for accurate *SNO*-Cys detection and mapping.

In this context, we have developed a method that enables global, facile, and high-throughput identification of endogenous *SNO*-Cys residues. *SNO*TRAP (*SNO* trapping by triaryl phosphine) is a direct tagging technique that allows enrichment and identification of *SNO*-proteins and their cognate *SNO*-sites. Hyperactivation of cyclin-dependent kinase-5 (Cdk5) by its activator peptide, p25, leads to AD-like neurodegenerative pathology, and inhibition of p25 activity ameliorates AD phenotypes (18–20). The CK-p25 mouse model of AD-like neurodegeneration allows temporal characterization of neurodegeneration through inducible expression of the p25 activator peptide, leading to elevated amyloid-β levels and DNA damage, followed by synaptic loss, neuronal death, and cognitive impairments (21–24). *SNO*TRAP was used here to profile changes in the *SNO*-proteome of the CK-p25 mouse model of AD-like neurodegeneration and healthy controls (21, 22). Our data provide insights into signaling pathways that may be perturbed by *SNO* in the neurodegenerating brain that could provide novel avenues for AD-related therapies.

Results and Discussion

Site-Specific Identification of *SNO*-Peptides. *SNO*TRAP is a proteomic extension of the method described earlier for detecting low-molecular–weight RSNOs using phosphine ester reagents (25). The *SNO*TRAP probe consists of a triphenylphosphine thioester linked to a biotin molecule through a polyethyleneglycol (PEG) spacer group. The method is based on reaction of the triphenylphosphine thioester with RSNO and subsequent biotin-mediated affinity capture of labeled peptides and/or proteins. The probe reacts with *SNO* groups, first yielding an azaylide intermediate, which through a properly positioned electrophile (thioester), rearranges to form a disulfide–iminophosphorane (Fig. S1*A*) (25, 26). The reaction proceeds through a Staudinger ligation-type mechanism that retains the nitrogen atom and thiol moiety, allowing unequivocal confirmation of specific *SNO*-sites in the peptide. Overall, the workflow consists of three main steps: (*i*) blocking of reduced Cys residues with iodoacetamide (IAM), (*ii*) capture and release of *SNO*-proteins or *SNO*-peptides, and (*iii*) nanoflow liquid chromatography (nLC)–MS/MS analysis (Fig. 1*A*). Blocking with IAM prevents transnitrosation during sample preparation, ensuring that the in vivo location of *SNO*-sites is retained.

To identify *SNO* proteins, and their cognate *SNO*-sites, we used two complementary approaches (Fig. 1*A*). The first was to identify *SNO* proteins, whereby *SNO*TRAP-modified proteins were enriched by streptavidin affinity (Fig. 1*A*, *approach A*). Tryptic peptides were analyzed by LC–MS/MS, and proteins were identified by database searching. Identification of *SNO*-sites using approach A was hindered due to extra features in the mass spectra arising from the *SNO*TRAP tag. These features include (*i*) limited ionization due to the added bulkiness of the triphenylphosphine–PEG–biotin (*SNO*TRAP) tag, (*ii*) added features to the collision-induced dissociation (CID) spectra such as tag-related fragment ions and corresponding neutral losses, and (*iii*) ion suppression by the dominant ions created by the *SNO*TRAP tag.

Consequently, a second approach (B) was developed that substitutes *N*-ethyl maleimide (NEM) for the bulky *SNO*TRAP tag, which allows direct detection of *SNO*-sites by MS. Briefly, proteolytic digestion is performed before streptavidin capture to isolate modified peptide fragments that contain the *SNO*TRAP tag rather than intact *SNO*-proteins. (Fig. 1*A*, *approach B*). The *SNO*TRAP tag is subsequently cleaved, and the peptides eluted with triscarboxyethylphosphine (TCEP), and the liberated Cys labeled with NEM before nLC–MS/MS. This strategy selectively enriches only *SNO*-containing peptides, which reduces the complexity of the nLC separation and improves the detection of *SNO*-sites. The diagnostic fragment ions (DFIs) at m/z 126.0550, 125.0477, and 158.0276 verify that this was a *SNO*-peptide
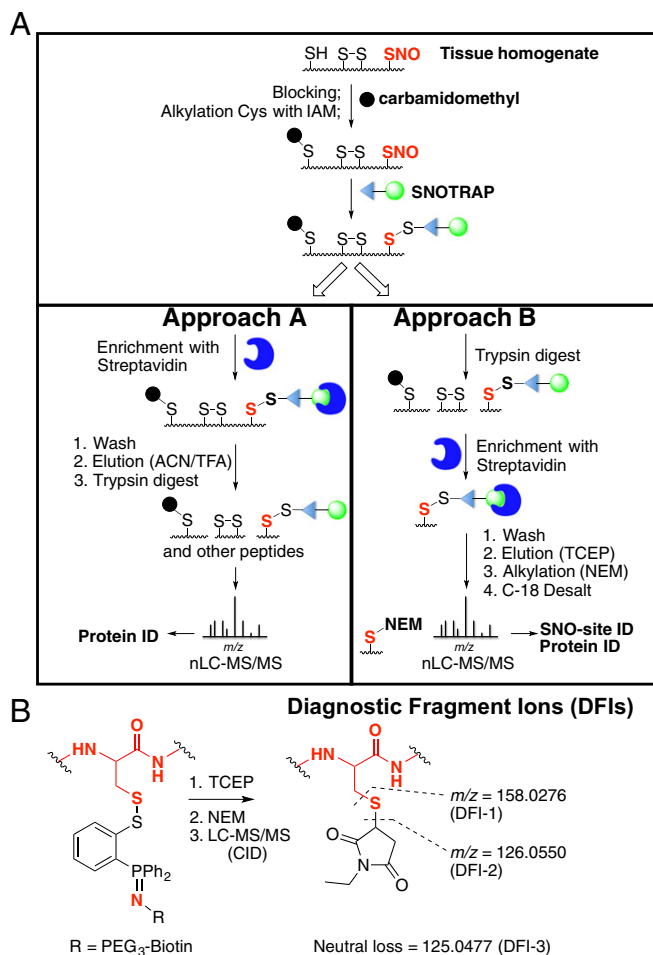
Fig. 1. Site-specific identification of *SNO*-protein. (*A*) Schematic for selective labeling and analysis of *SNO*-proteins. Unmodified Cys-thiols were blocked, and *SNO*-Cys sites were labeled with the *b-SNO*TRAP probe. For approach A, *b-SNO*TRAP–tagged proteins were enriched using streptavidin beads, washed, eluted with denaturing conditions, trypsin-digested, and analyzed by LC–MS/MS. For approach B, the proteome was trypsin-digested, and *b-SNO*TRAP–tagged peptides were enriched using streptavidin beads, followed by release of the biotin linker by TCEP; alkylated with NEM; and analyzed by LC–MS/MS. (*B*) Generation of DFIs from NEM-modified peptides.

(Fig. 1*B* and Fig. S1*B*) (27, 28). Our criteria for identification of *SNO*-proteins required detection of two or more tryptic peptides per *SNO*-protein using approach A and the *SNO*-Cys site-specific peptide identification using approach B.

Cortical tissues from CK-p25 mice were analyzed independently by capture of *SNO*-proteins (approach A) and *SNO*-peptides (approach B), using multiple biological replicates. Proteins were identified by Spectrum Mill (Agilent) for both approaches and pooled for analysis. By matching peptides for a given protein using a combination of both approaches, we identified 251 proteins (Dataset S1). DFIs in MS/MS spectra using approach B pinpointed 313 *SNO*-sites within these proteins (Dataset S1; MS/MS spectra can be viewed at web.mit.edu/toxms/www/SNOTRAP/). Detection of *SNO*-glyceraldehyde-3-phosphate dehydrogenase (GAPDH) on Cys-150, as previously reported by others using independent approaches, validated the robustness of the protocol (Fig. S1 *B* and *C*) (16, 29). *SNO*TRAP also detected previously unidentified *SNO*-sites, such as *SNO*-Cys284 of gephyrin (GPHN1), indicating the sensitivity of the method (Fig. S1 *B* and *C*). The *SNO*TRAP approach was able to detect and identify a large number of endogenous *SNO*-proteins and *SNO*-sites in the brain and is

complementary to previous reports for mouse, rat, and human (Fig. S1*F*) (16, 30–32).

To control for false positives that may result from nonspecific interactions with the streptavidin beads, pretreatment with TCEP, UV, and ascorbate-Cu were used to displace *SNO* PTMs before reaction with the *SNO*TRAP probe and analyzed by MS (Fig. S1*D*). Samples pretreated with TCEP were also analyzed by Western blot (Fig. S1*E*). Approximately 3% of peptides and 5% of proteins (*Materials and Methods*) were identified as false positives (present in both the test samples and negative controls) and were removed from further analysis.

SNO-Proteins Identified During Early Neurodegeneration. To determine temporal changes during neurodegeneration of *SNO*-proteins and their cognate *SNO*-Cys sites, we used the CK-p25 mouse model of AD-like neurodegeneration. CK-p25 mice show early signs of neurodegeneration, including DNA damage, increased amyloid-β, and the onset of neuroinflammation, before behavior abnormalities (Fig. 2*A*) (21, 22, 33). After 6 wk of p25 induction, mice exhibit learning and memory impairments and signs of advanced neurodegeneration, such as neuronal death and reduced synapse number (23, 24). To assess changes in *SNO* in the brain during the progression of neurodegeneration, we first measured GSNO levels in the hippocampus, cortex, and cerebellum of CK-p25 mice and p25 control littermates during early (2 wk) and later (6 wk) stages of neurodegeneration. In control mice, the levels of GSNO were highest in the cerebellum, reflecting previous observations that NOS1 expression is high in the cerebellum of adult mice (13). During early stages of neurodegeneration, GSNO increased in the cortex and the hippocampus to levels (twofold and threefold, respectively) that either resembled or surpassed that of the cerebellum (Fig. 2*B*). Increased *SNO* levels in 2-wk–induced CK-p25 mice correlate with elevated DNA damage previously observed in these regions (24). In the cerebellum, no increase in GSNO was observed at 2 wk, which likely reflects the low level of p25 induction in this brain region (21). GSNO levels in the hippocampus and cortex during a later stage of neurodegeneration return to levels similar to controls. Low levels of NO lead to *S*-nitrosation, whereas high levels cause cell death (14). The reduction of GSNO levels at a later stage of neurodegeneration could reflect a change in the proportion of cell types in these regions, including a loss of neurons and gliosis (21), although the possibility of lowered *SNO* production cannot be excluded. Collectively, our results suggest that elevated GSNO in the hippocampus and cortex is an early indicator of neurodegeneration and that elevated *SNO* may be a driving mechanism for disease progression.

To assess the endogenous *SNO*-proteome profile in the brains of CK-p25 and control mice during early stages of neurodegeneration (2 wk), *SNO*-proteins were isolated and identified in the cortex, hippocampus, and cerebellum. We detected a larger number of *SNO*-proteins and *SNO*-sites in CK-p25 mice compared with controls. In control mice, 152 *SNO*-sites and 116 *SNO*-proteins were identified, compared with 292 *SNO*-sites and 237 *SNO*-proteins in the CK-p25 mice (Dataset S1). The largest increase in CK-p25–specific *SNO*-proteins was detected in the cortex (Fig. 2*C*), which is consistent with elevated levels of GSNO during early neurodegeneration (Fig. 2*B*). Of the 212 *SNO*-proteins identified in the cortex, almost two-thirds (64%) were detected only in the CK-p25 mice (Fig. 2*C* and Dataset S1). A total of 264 *SNO*-Cys sites were identified in the cortex, of which 160 (61%) were found exclusively in CK-p25 mice (Dataset S1).

We detected 89 *SNO*-proteins in the hippocampus. Although AD pathology is readily observed in the hippocampus and our data show elevated GSNO, the majority of detected *SNO*-proteins (70%) were common between CK-p25 and controls (Fig. 2*C*). The reduced number of proteins may reflect a limitation in the total protein we obtained from the hippocampus (Fig. 2*C* and Dataset
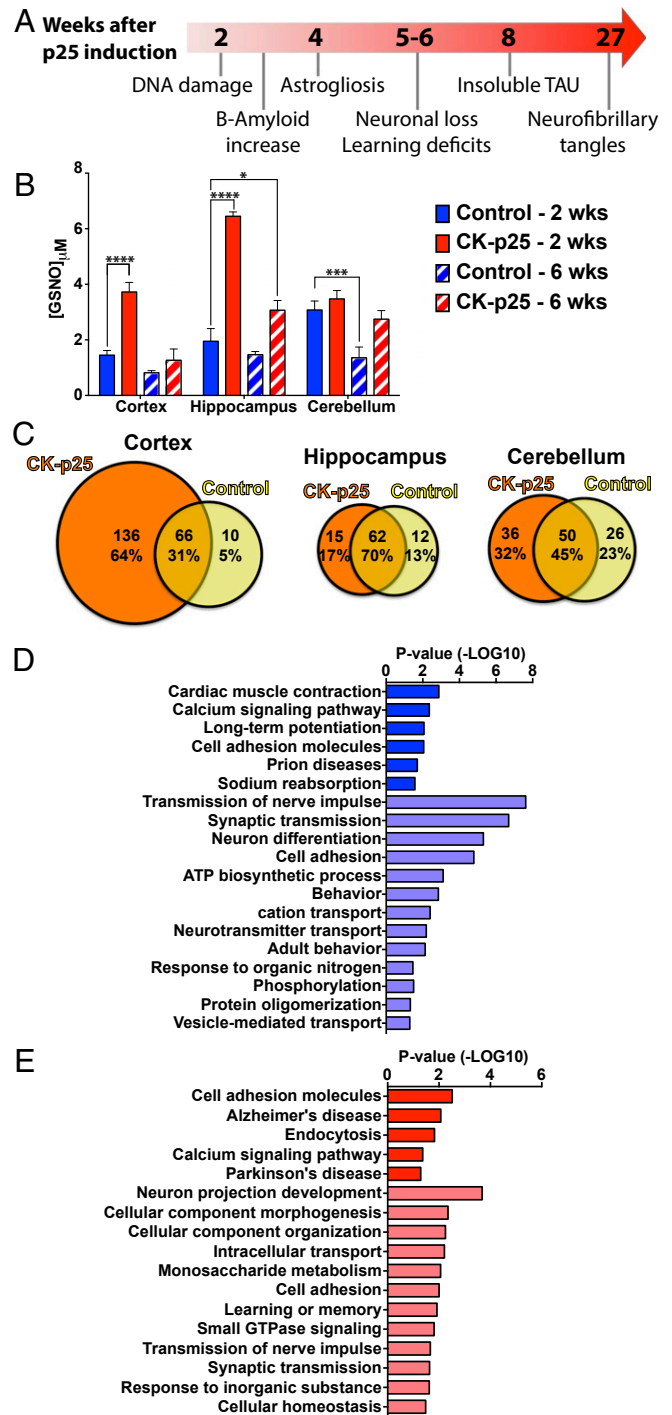
Fig. 2. Altered levels of *SNO* are detected in CK-p25 mice during early stages of neurodegeneration. (*A*) Timeline of the pathological progression of the CK-p25 mouse model of neurodegeneration. (*B*) GSNO concentration (μM) in the cortex, hippocampus, and cerebellum of control or CK-p25 mice following induction of p25 expression for 2 wk or 6 wk. Two-way ANOVA; Dunnett's multiple comparisons; ****$P < 0.0001$, ***$P < 0.001$, *$P < 0.05$; $n = 4$ for 2-wk samples and $n = 3$ for 6-wk samples; mean ± SEM. (*C*) Number of *SNO*-proteins identified in the cortex, hippocampus, and cerebellum of control and CK-p25 mice following 2-wk induction. (*D*) Gene ontology analysis of total *SNO*-proteins identified in the cortex of control mice (dark blue, KEGG pathways; light blue, BPs). (*E*) Gene ontology analysis of *SNO*-proteins exclusively identified in the cortex of CK-p25 mice following 2-wk induction (dark red, KEGG pathways; light red, BPs).
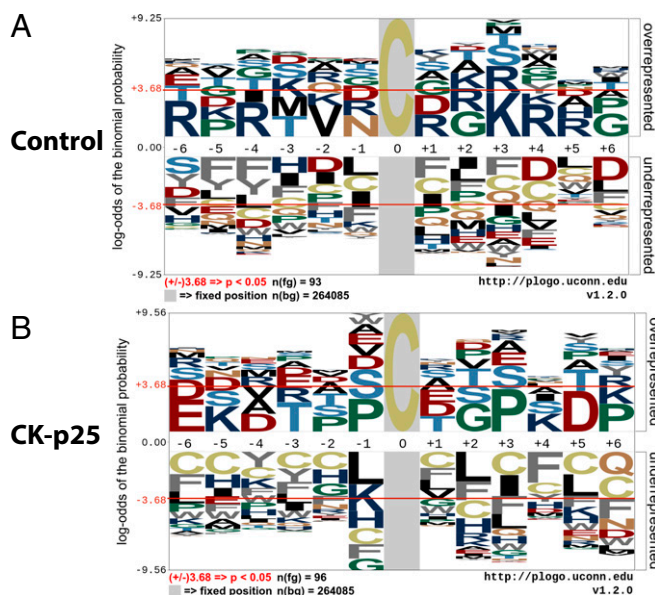
Fig. 3. *SNO*-site linear motif analysis indicates differential preference for *SNO*-Cys sites during early neurodegeneration. (*A*) Linear motif generated by pLOGO using sequences flanking *SNO*-Cys sites detected in control mice. (*B*) Linear motif generated by pLOGO using sequences flanking *SNO*-Cys sites exclusively detected in 2-wk–induced CK-p25 mice.

S1). The cerebellum has an approximately equal distribution of *SNO*-proteins (32%, 45%, and 23%) between control and CK-p25 mice (Fig. 2*C* and Dataset S1) and mirrors observations of little change in GSNO for this brain region (Fig. 2*B*).

Bioinformatic Analysis of the *S*-Nitrosoproteome. To decipher the possible impact of *SNO*-proteins on molecular and cellular systems during early neurodegeneration, we performed gene ontology analysis of biological processes (BPs) and KEGG pathways using the total control *SNO*-proteome (Fig. 2*D*) and the CK-p25–specific *SNO*-proteome (Fig. 2*E*) of the cortex (34, 35). Gene ontology clusters associated with synaptic functions were observed for *SNO*-proteins in control and CK-p25 mice (BP_Synaptic transmission and BP_Transmission of nerves impulse). The synaptic protein synaptophysin was validated by *SNO*TRAP-Western blot (Fig. S2*A*). Pathways associated with cognition were identified in both control (KEGG_Long-term potentiation and BP_Behavior) and CK-p25 mice (BP_Learning or memory). Collectively, these data suggest that regulation of synaptic *SNO*-proteins is important for normal neuronal functions associated with learning and memory and also that the synapse is vulnerable to aberrant *SNO*-signaling. NOS1, the major source of neuronal NO, is tethered to the synapse by postsynaptic density protein 95 (PSD95; also known as DLG4) (36). Although we did not detect *SNO*-PSD95 by MS, *SNO*TRAP-Western blot analysis shows a strong elevation of *SNO*-PSD95 in CK-p25 mice (Fig. S2*B*), indicating a susceptibility of the synapse to increased *SNO* during early neurodegeneration.

SNO-proteins linked to AD were detected in the CK-p25 cortex and not in controls, as identified by the AD KEGG pathway (Fig. 2*E*; GRIN2B, TAU, GSK3β, LRP1, NDUFS1, COX6B1, and GAPDH). NOS1 is activated by *N*-methyl-D-aspartate receptor (NMDAR)-mediated influx of Ca^{2+}; subsequent *S*-nitrosation of NMDAR is thought to modulate its activity. However, hyperexcitation of NMDAR leads to excessive Ca^{2+} signaling and elevated NO production, conditions thought to occur during neurodegeneration. This could explain detection of *SNO*-GRIN2B, a subunit of the NMDAR, in the CK-p25 mice. Amyloid activation

of the NMDAR can increase p25 production, possibly providing a feed-forward mechanism for *SNO* production (18). NMDAR-mediated p25 production and Cdk5 activation is thought to increase glycogen synthase kinase-3β (GSK3β) and TAU (Mapt) phosphorylation, two key mediators of neuronal death in AD, both of which we identified in the CK-p25 mice. Elevated *SNO*-GSK3β was validated by *SNO*TRAP-Western blot analysis (Fig. S2*A*). Cdk5 itself has been reported to be *S*-nitrosated, which enhances its serine/threonine kinase activity (37). Although *SNO*-Cdk5 was not detected by MS, it was elevated in CK-p25 mice (shown by *SNO*TRAP-Western blot; Fig. S2*B*), possibly contributing to elevated Cdk5 activity and acting as a feed-forward mechanism during neurodegeneration. In addition, protein kinase C (PKC) epsilon and gamma isoforms (Prkce and Prkcg) were *S*-nitrosated in CK-p25 mice. PKC inhibits GSK3β and promotes nonamyloidogenic processing of amyloid precursor protein (APP) through activation of α-secretase (38). *S*-nitrosation inhibits PKC activity (39, 40) and therefore may reduce APP processing through the nonamyloidogenic α-secretase pathway.

Additional AD-related pathways impacted by *SNO* during neurodegeneration included apolipoprotein E (ApoE)-mediated amyloid clearance (*SNO*-LRP1) and mitochondrial dysfunction (*SNO*-NDUFS1 and *SNO*-COX6B1, which are components of CxI and CxIV of the respiratory chain). Furthermore, Gene Ontology (GO) analysis indicated that proteins regulating glycolysis were enriched in the CK-p25–specific *SNO*-proteome (BP_Monosaccharide metabolism), suggesting that elevated *SNO* may affect metabolic processes during early neurodegeneration. In particular, GAPDH was *S*-nitrosated in CK-p25 mice but not in control mice and was validated by *SNO*TRAP-Western blot (Fig. S2*A*). Nuclear *SNO*-GAPDH transnitrosates SIRT1, HDAC2, and DNA-PK (DNA-dependent protein kinase, catalytic subunit), impacting metabolic pathways, aging, and chromatin remodeling (41–43). HDAC2 was not detected in our *SNO*-proteome, although we observed elevated *SNO*-HDAC2 in CK-p25 mice by *SNO*TRAP-Western blot (Fig. S2*B*).

Linear Motifs for *S*-Nitrosation. Recent studies indicate that the specificity of *SNO*-Cys sites may be dependent on the spatial proximity of charged amino acids, which are hypothesized to
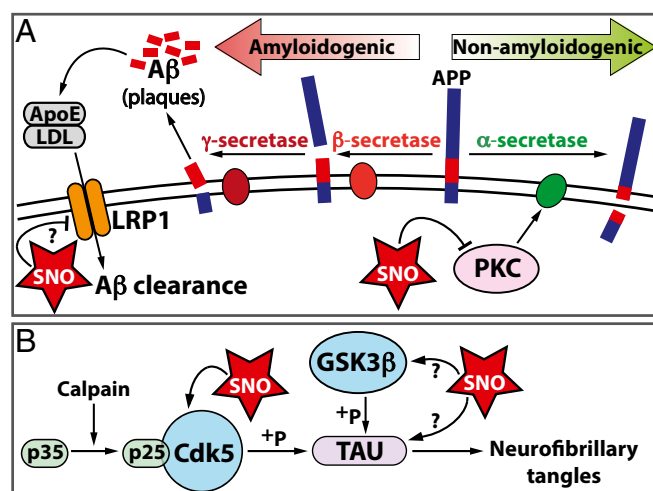
Fig. 4. Pathways affected by *S*-nitrosation during neurodegeneration. (*A*) *SNO*-LRP1 and *SNO*-PKC isoforms were identified in CK-p25 mice after 2-wk induction and have been implicated in secretase processing of APP and amyloid clearance. (*B*) *SNO*-GSK3β and *SNO*-TAU were identified in CK-p25 mice after 2-wk induction and have been implicated in neurofibrillary tangle formation and AD pathology. The functional implications of previously unidentified SNO-proteins are represented with a question mark.

allow protein–protein interactions that facilitate transnitrsation (29, 44). To elucidate common features of *SNO*-Cys sites, we used the probability LOGO (pLOGO) tool to analyze flanking sequences of *SNO*-Cys residues for linear motifs (45). Motif analysis of SNO-Cys sites in control and CK-p25 mice revealed an overrepresentation of charged flanking amino acids; however, this was not consistent for all SNO-Cys sites (Fig. 3 *A* and *B*). Specifically, in control mice, basic residues Arg (R) and Lys (K) were overrepresented at the –6, –4, +1, +3, +4, and +5 positions (Fig. 3*A*); these residues may be required for base-catalyzed transnitrosation (1, 46). To test the robustness of the motif, we performed pLOGO analysis using an independently published *SNO*-proteome from brains of wild-type (C57BL/6J) mice (47) and found an enrichment of the basic residues—Lys (K), Arg (R), and His (H)—surrounding the *SNO*-Cys position (Fig. S2*C*, –6, –5, –1, +3, and +4). In the CK-p25 mice, we observed Lys (K) basic residues at the –5 and +4 positions and Glu (E) and Asp (D) acidic residues at the –6, –4, and +5 positions (Fig. 3*B*). This motif may represent charge clustering and has been previously proposed to allow acid–base catalysis for nitrosation (base) and denitrosation (acid) of Cys residues. Despite these observations, many *SNO*-Cys sites identified in both control and CK-p25 mice did not have charged amino acids within a proximal location of the primary sequence. Previous studies indicate that tertiary structural elements may be required for localizing charged residues to SNO-Cys sites for many proteins (29, 44). Collectively, these data suggest that the specificity for *S*-nitrosation of a subset of Cys may be dependent on proximal charged amino acids, which possibly provide docking sites for nitrosating and denitrosating agents (29).

Conclusion

Through development of *SNO*TRAP, a direct *SNO*-tagging MS method for detecting both small and large molecular RSNOs, we identified an expanded endogenous *SNO*-proteome in the mouse brain. We identified the hippocampus and cortex as regions subjected to elevated levels of *SNO* during early stages of neurodegeneration that precede the onset of detrimental behavioral changes. The identification of *SNO*-PKC and *SNO*-LRP1 during neurodegeneration suggests that elevated *SNO* may impact amyloid processing and clearance, thus contributing to amyloid plaque deposition (Fig. 4*A*). Furthermore, detection of *SNO*-GSK3β and *SNO*-TAU in the CK-p25 mice indicates that aberrant *SNO* signaling may affect neurofibrillary tangle formation, another hallmark of AD pathology (Fig. 4*B*). The susceptibility of multiple proteins to *S*-nitrosation during early neurodegeneration relevant to synaptic function, metabolism, and AD pathology may drive cellular pathologies observed at later stages, such as neuronal loss, reduced synapse integrity, and ultimately memory impairment (Fig. 4 *A* and *B*). Increased protein aggregation and cell death linked to *SNO*-proteins in CK-p25 mice likely lead to activation of inflammatory responses, an important component of AD pathology and progression (33). The *SNO*TRAP strategy provided a comprehensive assessment of *S*-nitrosation in the neurodegenerating brain that can be applied to multiple cellular and disease contexts and has therapeutic potential for biomarker discovery and drug development.

Animals. All mouse experiments were approved by the Committee on Animal Care of the Division of Comparative Medicine at Massachusetts Institute of Technology.

1. Hess DT, Matsumoto A, Kim SO, Marshall HE, Stamler JS (2005) Protein S-nitrosylation: Purview and parameters. *Nat Rev Mol Cell Biol* 6(2):150–166.
2. Smith BC, Marletta MA (2012) Mechanisms of S-nitrosothiol formation and selectivity in nitric oxide signaling. *Curr Opin Chem Biol* 16(5-6):498–506.
3. Martínez-Ruiz A, Cadenas S, Lamas S (2011) Nitric oxide signaling: Classical, less classical, and nonclassical mechanisms. *Free Radic Biol Med* 51(1):17–29.
4. Keshive M, Singh S, Wishnok JS, Tannenbaum SR, Deen WM (1996) Kinetics of S-nitrosation of thiols in nitric oxide solutions. *Chem Res Toxicol* 9(6):988–993.
5. Keszler A, Zhang Y, Hogg N (2010) Reaction between nitric oxide, glutathione, and oxygen in the presence and absence of protein: How are S-nitrosothiols formed? *Free Radic Biol Med* 48(1):55–64.
6. Madej E, Folkes LK, Wardman P, Czapski G, Goldstein S (2008) Thiyl radicals react with nitric oxide to form S-nitrosothiols with rate constants near the diffusion-controlled limit. *Free Radic Biol Med* 44(12):2013–2018.
7. Mitchell DA, Marletta MA (2005) Thioredoxin catalyzes the S-nitrosation of the caspase-3 active site cysteine. *Nat Chem Biol* 1(3):154–158.
8. Seth D, Stamler JS (2011) The SNO-proteome: Causation and classifications. *Curr Opin Chem Biol* 15(1):129–136.
9. Nakamura T, et al. (2015) Aberrant protein S-nitrosylation contributes to the pathophysiology of neurodegenerative diseases. *Neurobiol Dis* 84:99–108.
10. Abbott A (2012) Cognition: The brain's decline. *Nature* 492(7427):S4–S5.
11. Agostinho P, Cunha RA, Oliveira C (2010) Neuroinflammation, oxidative stress and the pathogenesis of Alzheimer's disease. *Curr Pharm Des* 16(25):2766–2778.
12. Sultana R, Butterfield DA (2010) Role of oxidative stress in the progression of Alzheimer's disease. *J Alzheimers Dis* 19(1):341–353.
13. Bredt DS, Snyder SH (1994) Transient nitric oxide synthase neurons in embryonic cerebral cortical plate, sensory ganglia, and olfactory epithelium. *Neuron* 13(2):301–313.
14. Dedon PC, Tannenbaum SR (2004) Reactive nitrogen species in the chemical biology of inflammation. *Arch Biochem Biophys* 423(1):12–22.
15. Forrester MT, et al. (2009) Proteomic analysis of S-nitrosylation and denitrosylation by resin-assisted capture. *Nat Biotechnol* 27(6):557–559.
16. Hao G, Derakhshan B, Shi L, Campagne F, Gross SS (2006) SNOSID, a proteomic method for identification of cysteine S-nitrosylation sites in complex protein mixtures. *Proc Natl Acad Sci USA* 103(4):1012–1017.
17. Jaffrey SR, Erdjument-Bromage H, Ferris CD, Tempst P, Snyder SH (2001) Protein S-nitrosylation: A physiological signal for neuronal nitric oxide. *Nat Cell Biol* 3(2):193–197.
18. Seo J, et al. (2014) Activity-dependent p25 generation regulates synaptic plasticity and Aβ-induced cognitive impairment. *Cell* 157(2):486–498.
19. Shukla V, et al. (2013) A truncated peptide from p35, a Cdk5 activator, prevents Alzheimer's disease phenotypes in model mice. *FASEB J* 27(1):174–186.
20. Shukla V, Skuntz S, Pant HC (2012) Deregulated Cdk5 activity is involved in inducing Alzheimer's disease. *Arch Med Res* 43(8):655–662.
21. Cruz JC, Tseng H-C, Goldman JA, Shih H, Tsai L-H (2003) Aberrant Cdk5 activation by p25 triggers pathological events leading to neurodegeneration and neurofibrillary tangles. *Neuron* 40(3):471–483.
22. Cruz JC, et al. (2006) p25/cyclin-dependent kinase 5 induces production and intraneuronal accumulation of amyloid beta in vivo. *J Neurosci* 26(41):10536–10541.
23. Fischer A, Sananbenesi F, Pang PT, Lu B, Tsai L-H (2005) Opposing roles of transient and prolonged expression of p25 in synaptic plasticity and hippocampus-dependent memory. *Neuron* 48(5):825–838.
24. Kim D, et al. (2008) Deregulation of HDAC1 by p25/Cdk5 in neurotoxicity. *Neuron* 60(5):803–817.
25. Seneviratne U, Godoy LC, Wishnok JS, Wogan GN, Tannenbaum SR (2013) Mechanism-based triarylphosphine-ester probes for capture of endogenous RSNOs. *J Am Chem Soc* 135(20):7693–7704.
26. Zhang J, Wang H, Xian M (2009) An unexpected Bis-ligation of S-nitrosothiols. *J Am Chem Soc* 131(11):3854–3855.
27. Levsen K, et al. (2005) Structure elucidation of phase II metabolites by tandem mass spectrometry: An overview. *J Chromatogr A* 1067(1-2):55–72.
28. Yang J, Gupta V, Carroll KS, Liebler DC (2014) Site-specific mapping and quantification of protein S-sulphenylation in cells. *Nat Commun* 5:4776.
29. Doulias P-T, et al. (2010) Structural profiling of endogenous S-nitrosocysteine residues reveals unique features that accommodate diverse mechanisms for protein S-nitrosylation. *Proc Natl Acad Sci USA* 107(39):16958–16963.
30. Doulias P-T, Tenopoulou M, Greene JL, Raju K, Ischiropoulos H (2013) Nitric oxide regulates mitochondrial fatty acid metabolism through reversible protein S-nitrosylation. *Sci Signal* 6(256):rs1.
31. Zahid S, Khan R, Oellerich M, Ahmed N, Asif AR (2014) Differential S-nitrosylation of proteins in Alzheimer's disease. *Neuroscience* 256:126–136.
32. Zaręba-Kozioł M, Szwajda A, Dadlez M, Wysłouch-Cieszyńska A, Lalowski M (2014) Global analysis of S-nitrosylation sites in the wild type (APP) transgenic mouse brainclues for synaptic pathology. *Mol Cell Proteomics* 13(9):2288–2305.
33. Gjoneska E, et al. (2015) Conserved epigenomic signals in mice and humans reveal immune basis of Alzheimer's disease. *Nature* 518(7539):365–369.
34. Huang W, Sherman BT, Lempicki RA (2009) Systematic and integrative analysis of large gene lists using DAVID bioinformatics resources. *Nat Protoc* 4(1):44–57.
35. Mi H, Muruganujan A, Casagrande JT, Thomas PD (2013) Large-scale gene function analysis with the PANTHER classification system. *Nat Protoc* 8(8):1551–1566.

36. Christopherson KS, Hillier BJ, Lim WA, Bredt DS (1999) PSD-95 assembles a ternary complex with the N-methyl-D-aspartic acid receptor and a bivalent neuronal NO synthase PDZ domain. *J Biol Chem* 274(39):27467–27473.

37. Qu J, et al. (2011) S-Nitrosylation activates Cdk5 and contributes to synaptic spine loss induced by beta-amyloid peptide. *Proc Natl Acad Sci USA* 108(34):14330–14335.

38. de Barry J, Liégeois CM, Janoshazi A (2010) Protein kinase C as a peripheral biomarker for Alzheimer's disease. *Exp Gerontol* 45(1):64–69.

39. Choi H, Tostes RC, Webb RC (2011) Thioredoxin reductase inhibition reduces relaxation by increasing oxidative stress and s-nitrosylation in mouse aorta. *J Cardiovasc Pharmacol* 58(5):522–527.

40. Gopalakrishna R, Chen ZH, Gundimeda U (1993) Nitric oxide and nitric oxide-generating agents induce a reversible inactivation of protein kinase C activity and phorbol ester binding. *J Biol Chem* 268(36):27180–27185.

41. Hara MR, et al. (2005) S-nitrosylated GAPDH initiates apoptotic cell death by nuclear translocation following Siah1 binding. *Nat Cell Biol* 7(7):665–674.

42. Kornberg MD, et al. (2010) GAPDH mediates nitrosylation of nuclear proteins. *Nat Cell Biol* 12(11):1094–1100.

43. Nott A, Watson PM, Robinson JD, Crepaldi L, Riccio A (2008) S-Nitrosylation of histone deacetylase 2 induces chromatin remodelling in neurons. *Nature* 455(7211):411–415.

44. Marino SM, Gladyshev VN (2010) Structural analysis of cysteine S-nitrosylation: A modified acid-based motif and the emerging role of trans-nitrosylation. *J Mol Biol* 395(4):844–859.

45. O'Shea JP, et al. (2013) pLogo: A probabilistic approach to visualizing sequence motifs. *Nat Methods* 10(12):1211–1212.

46. Stamler JS, Toone EJ, Lipton SA, Sucher NJ (1997) (S)NO signals: Translocation, regulation, and a consensus motif. *Neuron* 18(5):691–696.

47. Raju K, et al. (2015) Regulation of brain glutamate metabolism by nitric oxide and S-nitrosylation. *Sci Signal* 8(384):ra68.

48. Block E, Ofori-Okai G, Zubieta J (1989) 2-phosphino- and 2-phosphinylbenzenethiols: New ligand types. *J Am Chem Soc* 111(6):2327–2329.

49. Figuly GD, Loop CK, Martin JC (1989) Directed ortho-lithiation of lithium thiophenolate. New methodology for the preparation of ortho-substituted thiophenols and related compounds. *J Am Chem Soc* 111(2):654–658.

50. Wiśniewski JR, Zougman A, Nagaraj N, Mann M (2009) Universal sample preparation method for proteome analysis. *Nat Methods* 6(5):359–362.

51. Slade PG, et al. (2010) Proteins modified by the lipid peroxidation aldehyde 9,12-dioxo-10(E)-dodecenoic acid in MCF7 breast cancer cells. *Chem Res Toxicol* 23(3):557–567.

52. Ravindra KC, et al. (2015) Untargeted proteomics and systems-based mechanistic investigation of artesunate in human bronchial epithelial cells. *Chem Res Toxicol* 28(10):1903–1913.

53. Huang DW, et al. (2007) The DAVID Gene Functional Classification Tool: A novel biological module-centric algorithm to functionally analyze large gene lists. *Genome Biol* 8(9):R183.

MEDICAL SCIENCES

Supporting Information

Seneviratne et al. 10.1073/pnas.1521318113

Materials and Methods

Reagents. Chemical reagents were obtained from commercial sources (Sigma-Aldrich for chemicals, Cambridge Isotope Laboratories for deuterated solvents, Isotec for $^{13}C_2,^{15}N$-labeled G*SH, Creative PEGWorks for maleimide–PEG–maleimide, and ChemPep, Inc., for biotin–PEG$_3$–propionic acid) and were used without additional purification. Sequencing-grade modified trypsin was obtained from Promega. Complete protease inhibitor mixture was from Sigma. Extraction and silica chromatography solvents were reagent grade. LC–MS and HPLC solvents were HPLC grade. Acetonitrile was distilled for HPLC and LC–MS. Distilled water was obtained in house and redistilled for HPLC and LC–MS experiments. Vivaspin 3,000, 10,000, and 30,000 molecular-weight cutoff (MWCO) membrane filters were from Sartorius Stedim NA. The primary antibodies used were as follows: Synaptophysin (Sigma, S5768), GAPDH (Cell Signaling Tech., 2118), Gsk3b (R&D), phosphatase and tensin homolog (PTEN) (Cell Signaling Tech., 9552), Cdk5 (Cell Signaling Tech., 2506), Stargazin (Santa Cruz, sc-374123), HDAC2 (Cell Signaling Tech., 2540), and PSD95 (NeuroMab, P78352). Secondary HRP-conjugated antibodies were purchased from Santa Cruz Biotechnology (sc-2030 and sc-2005). ECL reagent was from GE Healthcare (RPN2232). Unless otherwise stated, all sample preparations, nitrosothiol preparations, and *SNO*-probe reactions were carried out in the dark at room temperature. For NMR analysis, ^1H NMR spectra were recorded on Bruker Avance-600 and Varian Inova-500 instruments at 600.13 and 500.13 MHz, respectively. The ^{13}C NMR spectra were recorded on a Varian Inova-500 instrument operating at 125.76 MHz. ^{31}P NMR spectra were recorded on a Varian Inova-500 instrument operating at 202.46 MHz, and ^{31}P chemical shifts are relative to 3% (vol/vol) H_3PO_4 ($\delta = 0$ ppm) contained in a concentric internal capillary (Wilmad). NMR spectra were obtained using Bruker 5-mm TXI cryo-probes and Varian 5-mm pulsed-field gradient (PFG)-probes held at 22 °C unless otherwise stated.

Animals. All mouse experiments were approved by the Committee on Animal Care of the Division of Comparative Medicine at MIT. Adult (2.5–3 mo old) male double-transgenic CK-p25 mice and respective p25 control littermates were used (21). Tissue was collected at 2 or 6 wk after induction of p25 expression. Three brain regions were dissected from each mouse (cortex, hippocampus, and cerebellum). Dissections were performed on ice, immediately flash frozen in liquid nitrogen, and stored at –80 °C. Each biological replicate represents data obtained using tissue from an individual mouse. For the GNSO experiments, four biological replicates were used per group for 2-wk induction, and three biological replicates were used per group for 6-wk induction. For MS analysis, three biological replicates and two technical replicates were used per group for both method A and method B, and each sample was preseparated into five fractions.

Synthesis of *SNO*TRAP-Biotin. To a stirred 2-(diphenylphosphino)-benzenethiol (48, 49) (100 mg, 0.34 mmol) in dry DMF (5 mL) we added biotin–PEG$_3$–propionic acid (100 mg, 0.22 mmol; ChemPep, Inc.), N,N′-dicyclohexylcarbodiimide (70 mg, 0.34 mmol), and dimethylaminopyridine (4 mg, 0.03 mmol) successively. The resulting mixture was stirred for 7 h at room temperature, and the resulting clear solution was then concentrated under reduced pressure and purified by flash chromatography (hexane/EtOAc/MeOH gradient) to give the desired product (yield 30%). The *SNO*TRAP probe was repurified on an 1100 HPLC system with a photodiode array

UV detector at 254 nm (Agilent Technologies). HPLC columns and solvent systems were as follows: A semipreparative Phenomenex Luna C18 (25 cm × 9.4 mm, 10 µm) column was eluted with a linear gradient of 0.1% formic acid in water (A) and acetonitrile (B) at a flow rate of 2.5 mL/min. Solvent composition was initially at 40% for 5 min, 70% at 10 min, 90% at 20 min, and then further to 95% B over 8 min: ^1H NMR (500 MHz, CD$_3$CN, δ), 7.42–7.38 (m, 9H), 7.23–7.18 (m, 4H), 7.84 (m, 1H), 4.60–4.51 (m, 2H), 3.67–3.51 (m, 12H), 3.2 (m, 3H), 2.8 (m, 2H), 2.55 (t, 2H), 2.15 (t, 2H), 1.57–3.51 (m, 6H); ^{13}C NMR (125 MHz, CD$_3$CN, δ), 199.19, 172.5, 164.5, 144.8, 138.1, 137.0, 134.8, 129.9, 129.6, 129.6, 118.3, 69.2, 63.1, 62.3, 45.9, 42.5, 38.2, 27.1, 23.1, 22.5; ^{31}P NMR (202 MHz, CD$_3$CN, δ), −10.3; and HRMS-ESI$^+$ (m/z) [M + H$^+$]$^+$ calculated for $C_{37}H_{47}N_3O_6PS_2$, 724.2638, and found, 724.2632.

Sample Preparation for Tissue GSNO Analysis. Samples were first spiked with 500 fmol of isotopically labeled internal standard ($^{13}C_2,^{15}N$-labeled G*SNO) and mixed with maleimide–PEG–maleimide (20 mM, Creative PEGWorks) in PBS buffer containing 1 mM EDTA. For complete cell lysis, samples were subjected to three freeze/thaw cycles (dry ice to RT) with frequent vortexing. Lysed samples were kept 15 min at room temperature to allow complete blocking by maleimide-PEG-maleimide. Samples were centrifuged (16,000 × g, 10 min at 4 °C) to remove cell debris, followed by filtration using 3,000 MWCO membrane filters (15,000 × g, 15 min at 4 °C). The filtrate (low-molecular weight fraction) was then treated with the phosphine probe 3, as described in an earlier publication (3 mM final concentration, prepared by dissolving 4 mg of phosphine in 400 µL of 2:1 acetonitrile/methanol mixture) (25). The resulting clear solution was then freeze-dried to a final volume of 30 µL, and 8 µL was injected into the LC–MS/MS. To generate negative controls, the low molecular weight (LMW) filtrate was treated with 3 mM DTT (15 min, 24 °C).

Endogenous GSNO Quantification. LC–MS quantitation was performed by multiple-reaction monitoring (MRM), using the internal standard (G*SNO). A method calibration curve for LC–MS/MS was obtained by spiking 500 fmol of $^{13}C_2,^{15}N$-labeled internal standard (G*SNO) into the reaction between phosphine 3 (5 mM) and GSNO standards (0–10 pmol, in PBS buffer containing 1 mM EDTA). Regression analysis of the relative response ratio, calculated from LC–MS/MS peak area ratios corresponding, respectively, to analytes and internal standards, was then used to calculate the amount of GSNO (in pmols). This was then multiplied by 3.8 (total volume 30 µL/8 µL injection to a MS of 3.8) to obtain the total amount of analyte in the cell lysate. The GSNO concentration was determined by dividing the total amount of analyte (pmol) per million cells by the wet weight per million cells (mg), assuming that the wet weight of cells (10 million) was equal to the weight of water (i.e., 1 mg = 1 µL).

ESI$^+$–QqQ–MS Analyses. MRM and precursor-ion analyses were carried out in positive-ion mode, as described earlier (25), using an Agilent 1200 capillary HPLC system with an Agilent Triple Quad LC/MS (model 6430). The chromatography was done on an Agilent Eclipse XDB-C18 reverse-phase column (1.0 mm × 50 mm, 3.5 µm) with acetonitrile/water/formic acid gradients at 20 µL/min. The instrument parameters were optimized for maximum response during infusions of standard solutions.

Isolation and Preparation of Mouse Brain Protein Homogenates. Intact brains were collected, immediately frozen in liquid nitrogen, and stored at −80 °C. Isolated brain regions (cerebral cortex, hippocampus, and cerebellum) were homogenized into 3 mL lysis buffer (250 mM Hepes–NaOH, pH 7.7, containing 1 mM diethylene triamine pentaacetic acid, 0.1 mM neocuproine, 1% Triton X-100, 20 mM IAM, and protease inhibitors) on ice using a Teflon pestle and a Jumbo Stirrer (Fisher Scientific). The homogenates were centrifuged at 10,000 × g for 10 min at 4 °C. The soluble protein fraction was collected, and the protein concentration was determined by the Bradford assay. Each sample consisted of 2 mg of protein in 4 mL of lysis buffer (0.5 mg/mL). Lysates were then split into equal aliquots. Negative controls were generated by treatment with 10 mM TCEP for 30 min at room temperature or with Cu-ascorbate. Following treatment with 2.5% SDS (final) and 300 mM IAM in 250 mM Hepes, pH 7.7, buffer, samples were alkylated by incubation in a Thermomixer in the dark at 37 °C and shaking for 30 min. To minimize sample loss during sample processing, filter-aided sample preparation (FASP) was used to remove excess reagents and the MWCO filter was used as a reaction vessel (50). After alkylation, excess IAM reagents were removed by buffer exchange with 8 M urea three times and Milli-Q water once by centrifugation at 4,000 × g for 30 min at 4 °C with 10,000 MWCO spin filters (Sartorius Corporation).

Probe Labeling. SNOTRAP stock solutions [in 40% acetonitrile (ACN)] were added to all samples to reach a final concentration of 1.2 mM (in 25 mM Hepes buffer at pH 7.7) to selectively convert SNO to stable disulfide–iminophosphorane. Samples were incubated with SNOTRAP solution at room temperature for 2 h for complete labeling. Excess reagent was removed by three washes with 25 mM Hepes, pH 7.7, buffer and centrifuged at 4,000 × g for 30 min at 4 °C with 10,000 MWCO spin filters.

Streptavidin Affinity Chromatography of SNOTRAP-Derivatized SNO-proteins and Protein Digestion. Streptavidin was used to enrich for SNOTRAP-derivatized proteins according to the protocol detailed in Slade et al. (51). Briefly, following addition of the samples to the streptavidin columns, the columns were washed with PBS/CHAPS and distilled water, eluted with TFA/acetonitrile, and then frozen, lyophilized, and stored at –20 °C. In-solution protein digestion (in 25 mM Hepes, pH 7.7, buffer) for each sample was carried out in the dark at 37 °C for 3 h by adding 8.8 μg trypsin (sequencing grade-modified trypsin was obtained from Promega) and 1 mM CaCl$_2$ to each sample. The digests were transferred to 30-kDa cutoff filters (previously rinsed with methanol and washed with water) to remove trypsin and other higher molecular-weight components. Peptide-containing fractions were desalted using Agilent 100-μL C18 Bond Elut Zip tips and eluted with step gradients of acetonitrile fractions (20%, 40%, 60%, 80%, and 100%). Samples were reduced by Speedvac to less than 5 μL and adjusted to 10 μL with Millipore water. Eluted peptides (5 μL) were analyzed by LC–MS/MS, as described in *MS Analysis for Protein Identification*.

Protein Digestion and SNOTRAP-Biotin–Streptavidin Affinity Peptide Capture. For peptide-level enrichment, in-solution protein digestion (in 25 mM Hepes, pH 7.7, buffer) for each sample was carried out in the dark at 37 °C for 3 h by adding 8.8 μg trypsin and 1 mM CaCl$_2$ to each sample. The digests were transferred to 30-kDa cutoff filters (previously rinsed with methanol and washed with water) to remove trypsin and other higher molecular-weight components. The filtrate containing the biotinylated peptides was recovered and incubated with Neutravidin beads (200 μL slurry per milligram initial protein; washed with 10 volumes of 0.1 M ammonium bicarbonate) for 2 h at room temperature under

gentle rocking. Samples were centrifuged at 1,000 × g for 4 min, and the unbound fraction was removed. The beads were washed four times with 2.5 volumes of 1 M ammonium bicarbonate containing 50 mM NaCl, four times with 2.5 volumes of 0.1 M ammonium bicarbonate, two times with 2.5 volumes of 0.025 M ammonium bicarbonate, and finally four times with deionized water. Between each wash, beads were rocked for 2 min and centrifuged at 1,000 × g for 1 min. Bound peptides were eluted with 5 mM of TCEP by shaking for 30 min at room temperature. Eluted, Cys-containing peptides were alkylated using 100 mM NEM. Peptides containing fractions were desalted using Agilent 100-μL C18 Bond Elut Zip tips and eluted to a gradient of acetonitrile fractions (20%, 40%, 60%, 80%, and 100%). Samples were reduced in volume by Speedvac to less than 5 μL and adjusted to 10 μL with Millipore water. Eluted peptides (5 μL) were analyzed by LC–MS/MS, as described in *MS Analysis for Protein Identification*.

Western Blot Detection of Endogenous S-Nitrosoproteome in Mouse Brains. To detect endogenous SNO-proteins, control and CK/p25 samples were labeled using SNOTRAP as described above. Ultra-Link Immobilized Streptavidin beads (Thermo Scientific, 20349) (100 μL of slurry) were first washed with 25 mM Hepes buffer (pH 7.7) (3 × 200 μL), and probe-labeled proteins were added to the beads and pull-down was carried out for 1 h in pull-down buffer (25 mM Hepes, 150 mM NaCl, 0.05% SDS) at room temperature. Then beads were washed with (3 × 200 μL) wash buffer (25 mM Hepes buffer, pH 7.7, 0.1% SDS), (3 × 200 μL) 25 mM Hepes buffer (pH 7.7), and finally (2 × 200 μL) ddH$_2$O. Biotinylated proteins were eluted from beads by boiling in the presence of electrophoresis sample loading reducing buffer (contains DTT), followed by SDS/PAGE and transfer to polyvinylidene difluoride (PVDF) membranes. Membranes were blocked and incubated with monoclonal/polyclonal antibody, followed by respective secondary HRP-conjugated antibodies. Protein bands were visualized with ECL reagent, and bands were imaged using Fluorchem 8900 (Alpha Innotech). To detect endogenous SNO-biotinylated proteins, equal amounts of SNOTRAP-labeled proteins from control and CK/p25 samples (10 μg) were loaded into the SDS/PAGE gel for electrophoresis. The proteins were transferred into PVDF membranes, and the blot was probed against streptavidin–HRP to visualize total biotinylated proteins. The bands were captured using Fluorchem 8900 from Alpha Innotech. For negative controls, SNO modifications were reduced using TCEP and processed as with SNOTRAP labeling.

MS Analysis for Protein Identification. These were carried out on the Agilent HPLC-Chip/MS System, consisting of a micro-auto-sampler with a thermostat (set to 4 °C), a capillary and nanoflow pump with microdegasser, and the Chip-Cube that interfaces LC modules and the MS instrument. HPLC-grade water [0.1% formic acid (FA)] and ACN (0.1% FA) were used as mobile phases A and B, respectively. Separations were conducted on a Polaris-HR-Chip 3C18 (150 mm × 50 μm) 80A 3-μm C18 chip with 360 nL trap column (Agilent Technologies). Sample analysis used a 60-min gradient operating on the nanopump. The capillary pump provides a constant flow of 2 μL/min for delivery of samples from the autosampler to the HPLC–Chip interface. Two LC gradients were used. Mobile phases were 0.1% formic acid in HPLC-grade water (phase A) and 0.1% formic acid in acetonitrile (phase B). In MS approach A, the gradient started at 3% B at 300 nL/min for 5 min and increased to 30% B from 2 to 102 min, to 60% B at 112 min, to 90% B at 125 min, and to 97% at 126 min, was held for 4 min, and was followed by a 10-min postrun at 3% B. For MS approach B, the gradient started at 3% B at 300 nL/min for 5 min and increased to 30% B from 2 to 35 min, to 60% B at 40 min, to 90% B at 45 min, to 97% at 46 min, was held for 4 min, and was followed by a 10-min postrun at 3%

B. Mass detection was performed with an Agilent 6550 Accurate-Mass Ion Funnel QTOF Chip-MS System operated in positive-ion mode. Mass spectra were acquired in the 1,700 Da extended dynamic range mode (2 GHz) using the following settings: ESI capillary voltage, 1,960 V; fragmentor, 360 V; Octopole RF peak, 750 V; drying gas, 13 L/min; drying temperature, 225 °C. Data were acquired at a rate of 6 MS spectra per second and 3 MS/MS spectra per second in the mass ranges of m/z 295–1,700 for MS and 50–1,700 for MS/MS and stored in profile mode with a maximum of 20 precursors per cycle with a threshold of 5,000 ions in a precursor abundance-based scan speed in a peptide isotope model, with +2, +3, and above charge state preference, with active exclusion after 1 spectra, and released after 0.15 min. Fragmentation energy was applied at a slope of 3.0 V/100 Da with a 3.0 offset. Mass accuracy was maintained by using internal reference ion m/z 1221.9906, in positive mode.

Data Processing. Agilent MassHunter Workstation software was used for data acquisition and processing, and Agilent Spectrum Mill MS Proteomics Workbench was used for database searching, with the false discovery rate set at 1% (see Ravindra et al., 2015, for details) (52). The data were additionally processed with X!Tandem. Reverse/random database searches and manual inspection of spectra were used to validate the peptide/protein identifications. BSA standards were run daily for quality control. Three biological and two technical replicate experiments were performed, and detection of *SNO*-peptides in at least two was required for identification. In addition, our criteria for identification of *SNO*-proteins required detection of two or more tryptic peptides per *SNO*-protein using approach A and the *SNO*-Cys site-specific peptide identification using approach B. Using the Spectrum Mill search engine (B.04.00.127, Agilent Technologies), raw MS/MS spectra were processed to extract MS/MS spectra and searched against the SwissProt database. During searching, the following parameters were used: carbamidomethylation as a fixed modification; trypsin; maximum of two missed cleavages; precursor mass tolerance, ±20 ppm; product mass tolerance, ±50 ppm; and maximum ambiguous precursor charge, 4. Data were evaluated, and protein identifications were considered significant if the following confidence thresholds were met: protein score, >13; individual peptide scores of at least 10; and Scored Peak Intensity, 60%. For approach B (*SNO*-

site identification), methionine oxidation, *N*-ethylmaleimide on Cys, carbamidomethyl on Cys, *N*-ethylmaleimide + H_2O on Cys, and protein N terminus acetylation were set as variable PTMs. Minimal peptide length was set to six amino acids, and a maximum of two missed cleavages was allowed. Peptide sequence and fragmentation spectrum information were visualized using Scaffold software (v.3.6, Proteome Software, Inc.) with the imported peptide hits from Spectrum Mill.

Label-Free Quantitation Using Precursor Intensity with Scaffold Q+. Precursor intensity was used for the fold-change quantitation of common proteins detected in cortical and hippocampal samples. The method is to work backward from the peptides that have been identified through their MS/MS spectra and compare the intensities of the MS peaks from which they were derived. Precursor intensity quantitation is based on the principle that the area of the peak in the MS1 chromatogram provides a measure of the relative abundance of the corresponding peptide in the sample. Peptides are identified based on their MS/MS spectra, and then the corresponding MS1 peaks are identified in each LC–MS/MS run. The areas under these peaks are calculated and normalized, and their ratios are used as a measure of the relative abundance of the peptides in different samples by Scaffold Q$^+$ (Proteome Software, Inc.). Relative quantities of proteins are estimated by combining the precursor intensities of the constituent peptides. Using the quantitative values based on precursor intensity, fold changes were calculated by selecting control samples as the reference using Scaffold.

Bioinformatics. To assess functional enrichment, the lists of *SNO*-proteins were submitted to DAVID (https://david.ncifcrf.gov) (34, 53). "Fold enrichment" was defined as the number of proteins detected in the sample compared with the total number of proteins expected in the mouse or human proteome in each GO BP and pathway. P values for term enrichment were calculated using the right-sided hypergeometric test. GO and KEGG pathway enrichment ($P < 0.05$) analyses were performed by using the functional annotation tool in DAVID. The consensus sequence motifs of *SNO*-Cys were visualized by pLogo, a linear sequence prediction algorithm based on their statistical significance ($P < 0.05$). Motif_x was used to align the Cys-containing peptide sequence for pLogo analysis (45).

Fig. S1. Site-specific identification of *SNO*-protein. (*A*) Schematic for selective tagging of protein *S*-nitrosothiols using the biotin-*SNO*TRAP (*b*-SNOTRAP) probe. The *SNO*TRAP reagent directly reacts with the –*SNO* group to yield an azaylide intermediate, which rearranges to form the disulfide–iminophosporane compound. (*B*) Representative MS/MS spectra for *SNO*-Cys150 of GAPDH and *SNO*-Cys284 of GPHN (*SNO*-Cys is highlighted in red). (*C*) Representative MS1 spectrums of GAPDH (monoisotopic *m/z* 944.4688, MH[+]error 0.1 ppm) and GPHN (monoisotopic *m/z* 565.2814, MH[+] error 0.2 ppm) identified in cortex with low ppm mass error. (*D*) Representative total ion chromatograms (TICs) after *b*-SNOTRAP capture showing ion intensity of untreated (black), TCEP-treated (red), UV-treated (green), and ascorbate-Cu-treated (blue) samples. Chromatogram corresponding to TCEP treatment was plotted with a y axis offset of 1E4. (*E*) Representative Western blot of total *b*-SNOTRAP–captured proteins of untreated (cortex control) and TCEP-treated samples. (*F*) Current methodologies used for detection of *SNO*-peptides and *SNO*-Cys sites (16, 30–32).
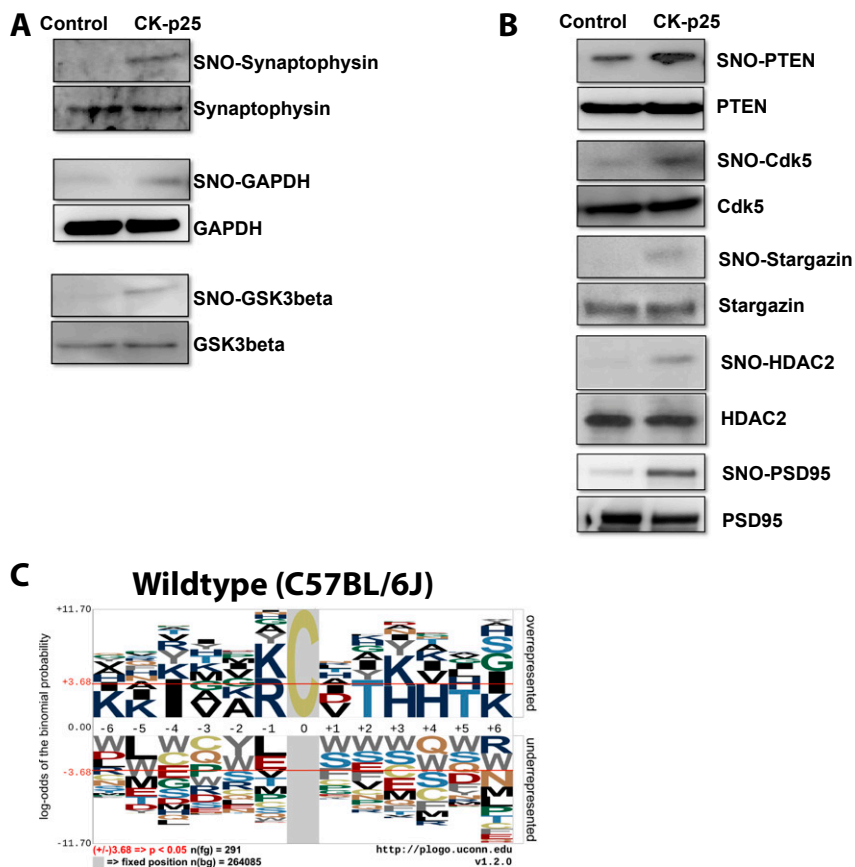
Fig. S2. Altered *SNO*-proteins during early neurodegeneration. (*A*) *SNO*-proteins identified by MS were validated by *SNO*TRAP Western blot analysis. Representative Western blot of *SNO*-Synaptophysin, *SNO*-GAPDH, and *SNO*-GSK3β in control and CK-p25 mice following 2-wk induction (*n* = 2). (*B*) Neuronal proteins previously identified as *S*-nitrosated that were not in our MS datasets were examined by *SNO*TRAP Western blot. Representative Western blot of *SNO*-PTEN, *SNO*-Cdk5, *SNO*-Stargazin, *SNO*-HDAC2, and *SNO*-PSD95 in control and CK-p25 mice following 2-wk induction (*n* = 2). (*C*) Linear motif generated by pLOGO using published sequences that flank *SNO*-Cys sites detected in C57BL/6 wild-type mice (47).

Other Supporting Information Files

Dataset S1 (PDF)

Table S1. *SNO*-proteins and *SNO*-Cys sites

Gene Symbol	UniprotKB Access #	Entry name	SPI %	SNO-Site	Sequence (# denotes *SNO*-Cys site)	Cortex CK-p25	Cortex Ctrl	Hipp CK-p25	Hipp Ctrl	Cerebellum CK-p25	Cerebellum Ctrl
Cnp	P16330	2',3'-cyclic-nucleotide 3'-phosphodiesterase	76.9	C111c	LDEDLAGY C# RR	✓		✓		✓	
Cnp	P16330	2',3'-cyclic-nucleotide 3'-phosphodiesterase	71.3	C157c	LD C# AQLKEK	✓					
Ado	Q6PDY2	2-aminoethanethiol dioxygenase	68.7	C225c	EASGSA C# DLPR	✓	✓	✓	✓		✓
Rps27l	Q6ZWY3	40S ribosomal proein S27-like	74.8	C77c	LTEG C# SFR	✓	✓	✓	✓		✓
Rps28	P62858	40S ribosomal protein S28	76.3	C27c	TGSQGQ C# TQVR			✓	✓		
Rpl10l	P86048	60S ribosomal protein L10-like	83.1	C195c	LIPDG C# GVK	✓	✓	✓	✓	✓	
Aco2	Q99KI0	Aconitate hydratase, mitochondrial	66.5	C385c	VGLIGS C# TNSSYEDMGR	✓				✓	
Adss	P46664	Adenylosuccinate synthetase isozyme 2		C18c	SISESSPAATSLPNDG C# GRPR	✓					
Arfgap1	Q9EPJ9	ADP-ribosylation factor GTPase-activating protein 1	69.9	C350c	SPSSDSWT C# ADASTGRR	✓					
Mllt4	Q9QZQ1	Afadin	72.2	C1700c	DYEPPSLSSAP C# APPPPPQR	✓					
Acan	Q61282	Aggrecan core protein	68.5	C220c	EG C# YGDKDEFPGVR	✓					
Cap1	P40124	adenylyl cyclase-associated protein 1	50.8	C426c	NSLDC# EIVSAK	✓					
Add1	Q9QYC0	Alpha-adducin	87.6	C430c	YSDVEVPASVTGHSFASDGDSGT C# SPLR	✓					
Add1	Q9QYC0	Alpha-adducin	67.3	C525c	TAGPQSQVL C# GVMMDR	✓					
Eno1	P17182	Alpha-enolase	83.7	C399c	TGAP C# RSER	✓		✓	✓	✓	✓
Fto	Q8BGW1	Alpha-ketoglutarate-dependent dioxygenase FTO	64.2	C184c	AGVGPS C# DDEVDLKSR	✓					
Man2c1	Q91W89	Alpha-mannosidase 2C1	56	C222c	SFQALHTANQMVNI C# DPAQPETYPAAK	✓					
Ank2	Q8C8R3	Ankyrin-2	70.2	C1538c	SGT C# MRDEGR	✓	✓	✓	✓	✓	
Amer2	Q8CCJ4	APC membrane recruitment protein 2	61.7	C665c	AAA C# HDSAK	✓		✓	✓		✓
Agap2	Q3UHD9	Arf-GAP with GTPase, ANK repeat and PH domain-containing protein 2	65.5	C805c	ALSTD C# TPSGDLSPLSR	✓					
As3mt	Q91WU5	Arsenite methyltransferase	58.3	C33c	TSADLQTNA C# VTR	✓					
Asphd1	Q2TA57	Aspartate beta-hydroxylase domain-containing protein 1	71.9	C95c	AGGVSGMPDV C# SQTGPR	✓					
Astn1	Q61137	Astrotactin-1	78.1	C278c	TLDSLQG C# NEK	✓	✓	✓			
Ntrk2	P15209	BDNF/NT-3 growth factors receptor	94.3	C176c	SSPDTQDLY C# LNESSK	✓	✓				
Ntrk2	P15209	BDNF/NT-3 growth factors receptor	72.2	C45c	IW C# TEPSPGIVAFPR	✓					
Hexb	P20060	Beta-hexosaminidase subunit beta	83.1	C288c	NLLTP C# YNQK	✓					
Hexb	P20060	Beta-hexosaminidase subunit beta	80.3	C530c	GIAAQPLYTGY C# NYENKI	✓					
Bcas1	Q80YN3	Breast carcinoma-amplified sequence 1 homolog	89.2	C389c	S C# SPPPPPPPEPTSEGR	✓	✓	✓	✓	✓	✓
Bcas1	Q80YN3	Breast carcinoma-amplified sequence 1 homolog	57.1	C574c	EPAP C# VQPPTVEANAMQTGDKTPK	✓	✓	✓	✓	✓	✓
Bcas1	Q80YN3	Breast carcinoma-amplified sequence 1 homolog	89.7	C318c	ADSV C# DGHAAGQK	✓	✓	✓	✓	✓	✓

Table S1. SNO-proteins and SNO-Cys sites. SNO-proteins and SNO-Cys sites detected in the cortex, hippocampus and cerebellum of control and CK-p25 mice. The ✔ symbol in the last column indicates the detection of the SNO-peptide using both Approach A and B according to tissue and genotype. SPI %, scored peak intensity obtained with Approach B. Hipp, hippocampus.

Table S1. *SNO*-proteins and *SNO*-Cys sites

Gene Symbol	UniprotKB Access #	Entry name	SPI %	SNO-Site	Sequence (# denotes *SNO*-Cys site)	Cortex CK-p25	Cortex Ctrl	Hipp CK-p25	Hipp Ctrl	Cerebellum CK-p25	Cerebellum Ctrl
Bcan	Q61361	Brevican core protein	93.5	C692c	SWEEAESQ C# R	✓	✓	✓	✓	✓	✓
Bcan	Q61361	Brevican core protein	67.9	C56c	IGATQLRGVLGGALAIP C# HVHHLRPPHSRR	✓					
C2cd5	Q7TPS5	C2 domain-containing protein 5	66.4	C884c	SAPP C# ASPTVGVVK	✓					
Pde1b	Q01065	Calcium/calmodulin-dependent 3',5'-cyclic nucleotide phosphodiesterase 1B	64.5	C16c	SPPEMLESD C# PSPLELK	✓					
Camkk1	Q8VBY2	Calcium/calmodulin-dependent protein kinase kinase 1	41.1	C122c	VAISDTED C# VQLNQYK	✓					
Camkk2	Q8C078	Calcium/calmodulin-dependent protein kinase kinase 2	72	C548c	AGP C# GGGGSALVK	✓	✓			✓	
Camk2a	P11798	Calcium/calmodulin-dependent protein kinase type II subunit alpha	88.3	C280c	STVAS C# MHR	✓	✓	✓	✓	✓	
Camk2a	P11798	Calcium/calmodulin-dependent protein kinase type II subunit alpha	59	C289c	QETVD C# LK	✓	✓	✓	✓	✓	
Camk2b	P28652	Calcium/calmodulin-dependent protein kinase type II subunit beta	71.1	C35c	L C# TGHEYAAK	✓		✓		✓	
Camsap2	Q8C1B1	Calmodulin-regulated spectrin-associated protein 2	76.8	C649c	EALSP C# PSTISTK	✓				✓	
Prkacb	P68181	cAMP-dependent protein kinase catalytic subunit beta	81.1	C349c	C# GKEF C# EF		✓				
Arpp21	Q9DCB4	cAMP-regulated phosphoprotein 21	93.3	C71c	SLAV C# EESSAR	✓	✓	✓	✓		
Cnr1	P47746	Cannabinoid receptor 1	79.3	C450c	AAES C# IKSTVK	✓	✓			✓	✓
Ca4	Q64444	Carbonic anhydrase 4	56.3	C35c	SS C# LGPEK					✓	✓
Ceacam1	P31809 Q925P2	Carcinoembryonic antigen-related cell adhesion molecule 1	81.5	C217c	TLTLLNVTRNDTGPYV C# ETR					✓	
Caskin1	Q6P9K8	Caskin-1	95.2	C1361c	AAASVVSGPPVASD C# ASPGDSAR	✓					
Ctnnd2	O35927	Catenin delta-2	70.5	C506c	QLQY C# ASVDSPYSK	✓					
Ctsl	P06797	Cathepsin L1	23	C211c	DGS C# KYR						✓
Cadm2	Q8BLQ9	Cell adhesion molecule 2	60	C248c	IIPSTPFPQEGGQALTLT C# ESK	✓					
Cadm3	Q99N28	Cell adhesion molecule 3	71.1	C150c	EKETATLN C# QSSGSKPAAQLTWR	✓				✓	
Cadm4	Q8R464	Cell adhesion molecule 4	83.0	C145c	EQAVEGGEVELS C# LVPR	✓					
Cnbp	P53996	Cellular nucleic acid-binding protein	61	C159c	TSEVN C# YR	✓	✓	✓	✓		✓
Cep170	Q6A065	Centrosomal protein of 170 kDa	80.8	C211c	SQEAGASG C# STEAK					✓	✓
Cep170	Q6A065	Centrosomal protein of 170 kDa	70.2	C625c	STS C# TTSLASQGER	✓	✓			✓	✓
Chmp5	Q9D7S9	Charged multivesicular body protein 5	70.2	C20c	APPPSLTD C# IGTVDSR	✓					
Cspg5	Q71M36	Chondroitin sulfate proteoglycan 5	85.4	C560c	LEGGKGDQDDLGVN C# LQNNLT	✓					
Clasp2	Q8BRT1	CLIP-associating protein 2	71.6	C968c	KEDGDTI C# SGPGMSDPR	✓					
Cfl1	P18760	Cofilin-1	76.9	C80c	MLPDKD C# R	✓	✓	✓	✓	✓	✓
Csde1	Q91W50	Cold shock domain-containing protein E1	56.1	C106c	MNGQVV C# AVPHNLESK	✓					

Table S1. SNO-proteins and SNO-Cys sites. SNO-proteins and SNO-Cys sites detected in the cortex, hippocampus and cerebellum of control and CK-p25 mice. The ✔ symbol in the last column indicates the detection of the SNO-peptide using both Approach A and B according to tissue and genotype. SPI %, scored peak intensity obtained with Approach B. Hipp, hippocampus.

Table S1. *SNO*-proteins and *SNO*-Cys sites

Gene Symbol	UniprotKB Access #	Entry name	SPI %	SNO-Site	Sequence (# denotes *SNO*-Cys site)	Cortex CK-p25	Cortex Ctrl	Hipp CK-p25	Hipp Ctrl	Cerebellum CK-p25	Cerebellum Ctrl
Cplx1	P63040	Complexin-1	70.7	C105c	KAIPPG C# GDEPEEEDESILDTVIK	✓					
Cplx2	P84086	Complexin-2	86.8	C90c	AALEQP C# EGSLTRPK	✓	✓		✓	✓	✓
Cntn1	P12960	Contactin-1	80.3	C65c	VSLN C# R			✓	✓	✓	
Cntnap1	O54991	Contactin-associated protein 1	81.8	C1251c	VQGELSESN C# GAMPR	✓	✓				
Cpne6	Q9Z140	Copine-6	64.7	C66c	S C# SSPVFSR			✓	✓		
Coro1c	Q9WUM4	Coronin-1C	71.1	C424c	SELS C# APK		✓	✓			
Cul2	Q9D4H8	Cullin-2	62.3	C266c	VIHE C# QQR			✓			
Uqcrh	P99028	Cytochrome b-c1 complex subunit 6, mitochondrial	87.9	C51c	LEL C# DNR	✓	✓	✓	✓	✓	✓
Uqcrh	P99028	Cytochrome b-c1 complex subunit 6, mitochondrial	74.2	C79c	DH C# VAHK	✓	✓	✓	✓	✓	✓
Uqcrh	P99028	Cytochrome b-c1 complex subunit 6, mitochondrial	64.6	C35c	EH C# EQLEK	✓	✓	✓	✓	✓	✓
Cox6b1	P56391	Cytochrome c oxidase subunit 6B1	72.2	C54c	GGDVSV C# EWYR	✓					
Hccs	P53702	Cytochrome c-type heme lyase	82.8	C70c	AYDYVE C# PVTGAR	✓					
Cyfip2	Q5SQX6	Cytoplasmic FMR1-interacting protein 2	82.5	C1253c	C# FQPPIHQSLATT C#	✓					
Dmtn	Q9WV69	Dematin	59.2	C84c	E C# SLSPK			✓			
Dsg1a	Q61495	Desmoglein-1-alpha	56.9	C702c	nSMRE C# R			✓			
Dstn	Q9R0P5	Destrin	58	C23c	C# STPEEIKKR					✓	
Rasd1	O35626	Dexamethasone-induced Ras-related protein 1	72.8	C214c	VSVQY C# DVLHkk	✓					
Dpysl2	O08553	Dihydropyrimidinase-related protein 2	96.9	C504c	GLYDGPV C# EVSVTPK	✓		✓	✓	✓	✓
Dlgap3	Q6PFD5	Disks large-associated protein 3	85.4	C103c C106c	MYPGQGPFDT C# ED C# VGHPQGK	✓				✓	
Dbnl	Q62418	Drebrin-like protein	76.8	C127c	AEEDVEPE C# IMEK	✓					
Map2k7	Q8CE90	Dual specificity mitogen-activated protein kinase kinase 7	57.5	C296c	SAG C# AAYMAPER					✓	
Huwe1	Q7TMY8	E3 ubiquitin-protein ligase HUWE1	58.4	C3361c	TKETN C# ESDRER	✓					
Nedd4	P46935	E3 ubiquitin-protein ligase NEDD4	90.6	C365c	LAV C# GNPATSQPVTSSNHSSR	✓				✓	
Erc1	Q99MI1	ELKS/Rab6-interacting/CAST family member 1	73.3	C258c	TGEP C# VAELTEENFQR	✓					
Eef1g	Q9D8N0	Elongation factor 1-gamma	91.4	C266c	AAAPAPEEEMDE C# EQALAAEPK	✓					
Tufm	Q8BFR5	Elongation factor Tu, mitochondrial	76.9	C127c	HYAHTD C# PGHADYVK	✓					
Gpr37l1	Q99JG2	Endothelin B receptor-like protein 2	87.1	C481c	ESPPLLPLGTP C#	✓	✓	✓	✓	✓	✓
Gpr37l1	Q99JG2	Endothelin B receptor-like protein 2	85.7	C203c	LLGDVS C# R	✓	✓	✓	✓	✓	✓
Edc3	Q8K2D3	Enhancer of mRNA-decapping protein 3	37.50	C137c	SQDVAISPQQQ C# SK	✓					
Echs1	Q8BH95	Enoyl-CoA hydratase, mitochondrial	73.8	C111c	TFQD C# YSSK			✓			

Table S1. SNO-proteins and SNO-Cys sites. SNO-proteins and SNO-Cys sites detected in the cortex, hippocampus and cerebellum of control and CK-p25 mice. The ✔ symbol in the last column indicates the detection of the SNO-peptide using both Approach A and B according to tissue and genotype. SPI %, scored peak intensity obtained with Approach B. Hipp, hippocampus.

Table S1. *SNO*-proteins and *SNO*-Cys sites

Gene Symbol	UniprotKB Access #	Entry name	SPI %	SNO-Site	Sequence (# denotes *SNO*-Cys site)	Cortex CK-p25	Cortex Ctrl	Hipp CK-p25	Hipp Ctrl	Cerebellum CK-p25	Cerebellum Ctrl
Epha6	Q62413	Ephrin type-A receptor 4	59.2	C4c	TAAGYGDFSEPLEV	✓	✓				
Slc1a3	P56564	Excitatory amino acid transporter 1	57.3	C375c	C# LEENNGVDKR					✓	✓
Slc1a2	P43006	Excitatory amino acid transporter 2	94.8	C561c	SAD C# SVEEEPWKRE	✓	✓	✓	✓	✓	✓
Fbxl16	A2RT62	F-box/LRR-repeat protein 16	87.4	C47c	NRP C# QPPPPPTLPPPSLATPLSR	✓					
Fxyd7	P59648	FXYD domain-containing ion transport regulator 7	65.8	C66c	S C# KSELPSSAPGGGGV	✓					
Gprin1	Q3UNH4	G protein-regulated inducer of neurite outgrowth 1	72.3	C174c	VDMP C# SSKVDIVSPGGDNAGSLR	✓					
Eno2	P17183	Gamma-enolase	60.5	C399c	TGAP C# RSER			✓	✓		
Gja1	P23242	Gap junction alpha-1 protein	75.8	C298c	LVTGDRNNSS C# R	✓	✓	✓	✓	✓	✓
Gja1	P23242	Gap junction alpha-1 protein	80.5	C260c	SDPYHATTGPLSPSKD C# GSPK	✓				✓	
Gphn	Q8BUV3	Gephyrin	79.9	C284c	LSTAS C# PTPK	✓		✓		✓	✓
Grid2	Q61625	Glutamate receptor ionotropic, delta-2	76.1	C131c	SG C# GLTR					✓	✓
Grin1	P35438	Glutamate receptor ionotropic, NMDA 1	71.4	C798c	YQE C# DSR	✓	✓	✓	✓		✓
Grin2b	Q01097	Glutamate receptor ionotropic, NMDA 2B	60.2	C436c	NTVP C# QKR	✓		✓	✓		
Gfpt1	P47856	Glutamine-fructose-6-phosphate aminotransferase 1	35.7	C262c	VDSTT C# LFPVEEK	✓					
Glul	P15105	Glutamine synthetase	90.2	C49c	TLD C# EPK	✓	✓	✓	✓	✓	✓
Gapdh	P16858	Glyceraldehyde-3-phosphate dehydrogenase	89.7	C150c	IVSNAS C# TTN C# LAPLAK	✓		✓		✓	✓
Gsk3b	Q9WV60	Glycogen synthase kinase-3 beta	56.7	C14c	TTSFAES C# KPVQQPSAFGSMK	✓					
Gpc1	Q9QZF2 P51655 Q9R087	Glypican-1	65	C32c	S C# SEVR		✓				
Gprasp1	Q5U4C1	G-protein coupled receptor-associated sorting protein 1	64.5	C535c	SVGVN C# EkMPK	✓	✓	✓	✓	✓	✓
Gnao1	P18872	Guanine nucleotide-binding protein G(o) subunit alpha	76.6	C108c	MV C# DVVSR	✓		✓		✓	
Hpx	Q91X72	Hemopexin	70.9	C458c	SLPQPQKVNSILG C# SQ	✓					
Hdgf	P51859	Hepatoma-derived growth factor	76.3	C12c	QKEYK C# GDLVFAK					✓	
Hpcal1	P62748	Hipocalcin-like protein 1	55.3	C185c	LLQ C# DPSSASQF	✓			✓		✓
Homer3	Q99JP6	Homer protein homolog 3	79	C311c	SME C# NLEEAR					✓	✓
Hapln1	Q9QUP5	Hyaluronan and proteoglycan link protein 1	78.4	C327c	C# SPTEAAVR		✓	✓	✓		
N/A	P01837	Ig kappa chain C region	56.4	C106c	SFNRNE C#	✓					
Igsf21	Q7TNR6	Immunoglobulin superfamily member 21	76.9	C116c	ISDNGPYE C# HVGIYDR	✓					
Igsf8	Q8R366	Immunoglobulin superfamily member 8	58.6	C184c	LTVHEGQELALG C# LAQTK	✓				✓	
Itpka	Q8R071	Inositol-trisphosphate 3-kinase A	55.2	C19c	GAGP C# SPGLER	✓					
Itgav	P43406	Integrin alpha-V	52.3	C172c	TVEYAP C# R			✓			

Table S1. SNO-proteins and SNO-Cys sites. SNO-proteins and SNO-Cys sites detected in the cortex, hippocampus and cerebellum of control and CK-p25 mice. The ✔ symbol in the last column indicates the detection of the SNO-peptide using both Approach A and B according to tissue and genotype. SPI %, scored peak intensity obtained with Approach B. Hipp, hippocampus.

Table S1. *SNO*-proteins and *SNO*-Cys sites

Gene Symbol	UniprotKB Access #	Entry name	SPI %	SNO-Site	Sequence (# denotes *SNO*-Cys site)	Cortex CK-p25	Cortex Ctrl	Hipp CK-p25	Hipp Ctrl	Cerebellum CK-p25	Cerebellum Ctrl
Icam5	Q60625	Intercellular adhesion molecule 5	94	C607c	VE C# VGSEGASEGIVLPLVSSNSGPR	✓	✓	✓	✓		
Icam5	Q60625	Intercellular adhesion molecule 5	63.8	C431c	SWTWPEGPEQTLH C# EAR	✓					
Icam5	Q60625	Intercellular adhesion molecule 5	56.6	C551c	C# EAINAR		✓		✓		
Icam5	Q60625	Intercellular adhesion molecule 5	80.7	C724c	C# VATNAHGTDSR	✓	✓	✓	✓		
Icam5	Q60625	Intercellular adhesion molecule 5	92.1	C415c	LDDLD C# PR	✓	✓	✓	✓		
Iqsec1	Q8R0S2	IQ motif and SEC7 domain-containing protein 1	82	C904c	A C# LDDSYASGEGLKR	✓					
Iqsec2	Q5DU25	IQ motif and SEC7 domain-containing protein 2	56.8	C616c	QLVYEADG C# SPHGTLK	✓					
Iscu	Q9D7P6	Iron-sulfur cluster assembly enzyme ISCU, mitochondrial	65.3	C70c	NVGTGLVGAPA C# GDVMK	✓					
Asrgl1	Q8C0M9	Isoaspartyl peptidase/L-asparaginase	77.2	C317c	LQAGIDL C# ETR	✓	✓	✓	✓	✓	✓
Asrgl1	Q8C0M9	Isoaspartyl peptidase/L-asparaginase	85.9	C179c	GAQNAD C# PK	✓	✓	✓	✓	✓	✓
Asrgl1	Q8C0M9	Isoaspartyl peptidase/L-asparaginase	75.4	C326c	TRDLP C#	✓	✓	✓	✓	✓	✓
Krt17	Q9QWL7	Keratin, type I cytoskeletal 17	60.1	C29c C40c	TS C# RLSGSLGAGS C# R	✓					✓
Krt81	Q9ERE2 P97861	Keratin, type II cuticular Hb1 (Fragment)	55.3	C210c	TK C# EEIk					✓	
Fn3krp	Q8K274	Ketosamine-3-kinase	63.8	C24c	ATGHSGGG C# ISQGQSYDTDKGR					✓	
Khdrbs1	Q60749	KH domain-containing, RNA-binding, signal transduction-associated protein 1	83.7	C19c	S C# SKDPSGAHPSVR	✓	✓	✓	✓	✓	✓
Kcp	Q3U492	Kielin/chordin-like protein	76.9	C278c	I C# Q C# LEGHIQ C# R	✓					
Kif1a	P33173	Kinesin-like protein KIF1A	68.2	C609c	TP C# AETPAEPVDWAFAQR	✓					
Lama1	P19137	Laminin subunit alpha-1	66.4	C3038c	QN C# LSSR				✓		
Llgl1	Q80Y17	Lethal(2) giant larvae protein homolog 1	68.3	C190c	SVPDDYR C# GK						✓
Luzp1	Q8R4U7	Leucine zipper protein 1	87.7	C561c	GQVPGHASQGTQAVESS C# SK					✓	
Lgi1	Q9JIA1	Leucine-rich glioma-inactivating protein 1	70.7	C55c	DNAL C# ENAR	✓		✓	✓	✓	
Lgi3	Q8K406	Leucine-rich repeat LGI family member 3	76	C52c	DTAF C# VDSK		✓			✓	✓
Rltpr	Q3V3V9	Leucine-rich repeat-containing protein 16C	71.2	C1227c	TSPAPDILSLPEDP C# LGPR	✓					
Lrrc7	Q80TE7	Leucine-rich repeat-containing protein 7	69.7	C541c	SM C# APLPVAAQSTTLPSLSGR	✓					
Lsamp	Q8BLK3	Limbic system-associated membrane protein	76.2	C239c	C# EASAVPAPDFEWYRDDTR		✓				✓
Lsamp	Q8BLK3	Limbic system-associated membrane protein	78.7	C197c	EQSGKYE C# K	✓	✓	✓	✓	✓	✓
Lppr4	Q7TME0	Lipid phosphate phosphatase-related protein type 4	84.7	C605c	NAEGSTVT C# TGSIR	✓	✓	✓	✓		
Lppr4	Q7TME0	Lipid phosphate phosphatase-related protein type 4	66.7	C569c	TVA C# NR	✓	✓	✓	✓		
Ldha	P06151	L-lactate dehydrogenase A chain	77.8	C84c	IVSSKDY C# VTANSK			✓	✓	✓	

Table S1. SNO-proteins and SNO-Cys sites. SNO-proteins and SNO-Cys sites detected in the cortex, hippocampus and cerebellum of control and CK-p25 mice. The ✔ symbol in the last column indicates the detection of the SNO-peptide using both Approach A and B according to tissue and genotype. SPI %, scored peak intensity obtained with Approach B. Hipp, hippocampus.

Table S1. *SNO*-proteins and *SNO*-Cys sites

Gene Symbol	UniprotKB Access #	Entry name	SPI %	SNO-Site	Sequence (# denotes *SNO*-Cys site)	Cortex CK-p25	Cortex Ctrl	Hipp CK-p25	Hipp Ctrl	Cerebellum CK-p25	Cerebellum Ctrl
Acsl4	Q9QUJ7	Long-chain-fatty-acid--CoA ligase 4	66.7	C157c	NTIAIF C# ETR	✓					
Prnp	P04925	Major prion protein	94.5	C213c	VVEQM C# VTQYQK	✓	✓		✓	✓	✓
Mdh1	P14152	Malate dehydrogenase, cytoplasmic	74.9	C154c	SAPSIPKENFS C# LTR	✓					
Madd	Q80U28	MAP kinase-activating death domain protein	83.6	C763c	QTETGEGSV C# QR	✓	✓	✓	✓		✓
Map7d1	A2AJI0	MAP7 domain-containing protein 1	84.2	C375c	SASASPLTP C# SAPR	✓	✓			✓	✓
Map1a	Q9QYR6	Microtubule-associated protein 1A	93.9	C2165c	SAP C# GSLAFSGDR	✓	✓		✓		✓
Map1a	Q9QYR6	Microtubule-associated protein 1A	55.4	C2058c	APISLSQDPSPPLNGSTTS C# GPDRR	✓					
Map1b	P14873	Microtubule-associated protein 1B	93.6	C1913c	TIKSP C# DSGYSYETIEK	✓	✓			✓	✓
Map1b	P14873	Microtubule-associated protein 1B	91.9	C1936c	TIKTPEDGGYT C# EITEK	✓					✓
Map1b	P14873	Microtubule-associated protein 1B	79.5	C1224c	SALRDAY C# SEEKELK	✓					
Map1b	P14873	Microtubule-associated protein 1B	61.8	C2037c	SPDTSAY C# YETMEK	✓	✓				
Map1b	P14873	Microtubule-associated protein 1B	55	C2061c	TPQASTYSYETSDR C# YTTEK	✓					
Map1a	Q9QYR6	Microtubule-associated protein 1a	73.1	C2165c	SAP C# GSLAFSGDR	✓	✓		✓		✓
Map2	P20357	Microtubule-associated protein 2	62.7	C759c	MP C# FPIESKEEEDKAEQAK	✓					
Map6	Q7TSJ2	Microtubule-associated protein 6	80	C500c	SLYSEPFKE C# PKVEKPSVQSSKPK			✓			
Mapre3	Q6PER3	Microtubule-associated protein RP/EB family member 3	71.8	C182c	LSNVAPP C# ILRKNPPSAR	✓		✓			
Mapt	P10637	Microtubule-associated protein tau	61.3	C151c	EAT C# QPSGTRPEDIEK	✓					✓
Mtch2	Q791V5	Mitochondrial carrier homolog 2	79.5	C296c	TY C# YDLR	✓	✓	✓	✓	✓	✓
Tomm40	Q9QYA2	Mitochondrial import receptor subunit TOM40 homolog	80.8	C74c	TPGAAASGAAAASEDGS C# G C# LPNPGTFEE C# HRK	✓					
Marc2	Q922Q1	MOSC domain-containing protein 2, mitochondrial	66.5	C74c	GVSV C# ETE C# TDMGLR	✓					
Rnmt	Q9D0L8	mRNA cap guanine-N7 methyltransferase	65.2	C37c	LPENTPP C# QQVDQPK	✓					
Muc6	Q80T03	Mucin-6	56.9	C966c	VLTENVI C# GkSGVT C# SR	✓					
Plp1	P60202	Myelin proteolipid protein	92.7	C201c	TSASIGSL C# ADAR	✓	✓	✓	✓	✓	✓
Plp1	P60202	Myelin proteolipid protein	75.2	C109c	TTI C# GK			✓			✓
Mag	P20917	Myelin-associated glycoprotein	61.9	C488c	VI C# TSR	✓		✓		✓	
Mog	Q61885	Myelin-oligodendrocyte glycoprotein	83.5	C52c	ALVGDEAELP C# R	✓					
Myadm	O35682	Myeloid-associated differentiation marker	74	C273c	SMDPS C# TR	✓		✓	✓	✓	
Ndufs1	Q91VD9	NADH-ubiquinone oxidoreductase 75 kDa subunit, mitochondrial	88.5	C727c	AVTEGAQAVEEPSI C#	✓					✓
Ganab	Q8BHN3	Neutral alpha-glucosidase AB	57.4	C41c C47c	T C# DESSF C# K	✓					
Ncam1	P13595	Neural cell adhesion molecule 1	95.4	C288c	NVDKNDEAEYV C# IAENK	✓	✓	✓	✓		✓

Table S1. SNO-proteins and SNO-Cys sites. SNO-proteins and SNO-Cys sites detected in the cortex, hippocampus and cerebellum of control and CK-p25 mice. The ✔ symbol in the last column indicates the detection of the SNO-peptide using both Approach A and B according to tissue and genotype. SPI %, scored peak intensity obtained with Approach B. Hipp, hippocampus.

Table S1. *SNO*-proteins and *SNO*-Cys sites

Gene Symbol	UniprotKB Access #	Entry name	SPI %	SNO-Site	Sequence (# denotes *SNO*-Cys site)	Cortex CK-p25	Cortex Ctrl	Hipp CK-p25	Hipp Ctrl	Cerebellum CK-p25	Cerebellum Ctrl
Ncam1	P13595	Neural cell adhesion molecule 1	80.2	C189c	TDEGTYR C# EGR		✓			✓	
Ncam2	O35136	Neural cell adhesion molecule 2	84.6	C380c	LSDSGRYD C# EAASR	✓					
Ncam2	O35136	Neural cell adhesion molecule 2	63.8	C136c	QGEDAEVV C# R	✓					
L1cam	P11627	Neural cell adhesion molecule L1	55	C353c	LD C# QVQGRPQPEITWR	✓	✓	✓	✓	✓	✓
Nrxn1	Q9CS84	Neurexin-1	56.2	C679c	QMAEIQSTAGVKPS C# SK	✓					
Ncald	Q91X97	Neurocalcin-delta	82.7	C185c	LLQ C# DPSSAGQF	✓					
Ncan	P55066	Neurocan core protein	83.5	C1167c	GTVL C# GPPPAVENASLVGVR	✓	✓				
Ncan	P55066	Neurocan core protein	66.8	C354c	FDAY C# FR	✓					
Ncan	P55066	Neurocan core protein	63	C279c	AQ C# QR	✓					
Ncdn	Q9Z0E0	Neurochondrin	81.9	C725c	MAALEQ C# LSEP	✓			✓		✓
Scg5	P12961	Neuroendocrine protein 7B2	62.1	C130c	TADDG C# LENAPDTAEFSR	✓					
Nfasc	Q810U3	Neurofascin	93.3	C118c	SGGRPEEYEGEYQ C# FAR	✓					
Nfasc	Q810U3	Neurofascin	81.2	C63c	DNILIE C# EAK	✓	✓		✓		✓
Nrgn	P60761	Neurogranin	73.1	C51c	SGE C# GRKGPGPGGPGGAGGAR	✓	✓	✓	✓	✓	✓
Nrgn	P60761	Neurogranin	94.8	C51c	SGE C# GR	✓	✓	✓	✓	✓	✓
Nrcam	Q810U4	Neuronal cell adhesion molecule	73.5	C519c	DSTGTYT C# VAR	✓	✓	✓	✓		✓
Nrcam	Q810U4	Neuronal cell adhesion molecule	85.3	C62c	ENIVIQ C# EAK	✓	✓	✓	✓		✓
Negr1	Q80Z24	Neuronal growth regulator 1	77.7	C197c	DQAGEYE C# SAENDVSFPDVKK	✓					
Hpca	P84075	Neuron-specific calcium-binding protein hippocalcin	86.3	C185c	LLQ C# DPSSASQF	✓					
Nptn	P97300	Neuroplastin	92.7	C116c	LTLEDSGTYE C# R	✓	✓	✓	✓	✓	✓
Nptn	P97300	Neuroplastin	84.9	C258c	SENKNEGQDAMMY C# K	✓	✓	✓	✓	✓	✓
Nptn	P97300	Neuroplastin	73.7	C217c	AEDSGEYH C# VYHFVSAPK	✓					
Ntm	Q99PJ0	Neurotrimin	93.5	C201c	EQSGEYE C# SASNDVAAPVVR	✓		✓			✓
Slc1a4	O35874 P56564	Neutral amino acid transporter A	90.7	C355c	C# IEENNGVDKR			✓	✓		✓
Ovch2	Q7M761	Ovochymase-2	60.5	C265c	GAWTLAGVTSWGLG C# GRSWRNnAR				✓		
Cask	O70589	Peripheral plasma membrane protein CASK	65.6	C684c	VA C# IAMEK				✓		
Prdx5	P99029	Peroxiredoxin-5, mitochondrial	75.4	C200c	ALNVEPDGTGLT C# SLAPNILSQ	✓					
Prdx6	O08709	Peroxiredoxin-6	91.3	C47c	DFTPV C# TTELGR	✓					
Pip5k1c	O70161	Phosphatidylinositol 4-phosphate 5-kinase type-1 gamma	56.7	C581c	ITVQVEPV C# GVGVVPK	✓	✓				
Phyhipl	Q8BGT8 Q8K0S0	Phytanoyl-CoA hydroxylase-interacting protein-like	64.5	C369c	T C# NISVGR	✓		✓	✓	✓	✓

Table S1. SNO-proteins and SNO-Cys sites. SNO-proteins and SNO-Cys sites detected in the cortex, hippocampus and cerebellum of control and CK-p25 mice. The ✔ symbol in the last column indicates the detection of the SNO-peptide using both Approach A and B according to tissue and genotype. SPI %, scored peak intensity obtained with Approach B. Hipp, hippocampus.

Table S1. *SNO*-proteins and *SNO*-Cys sites

Gene Symbol	UniprotKB Access #	Entry name	SPI %	SNO-Site	Sequence (# denotes *SNO*-Cys site)	Cortex CK-p25	Cortex Ctrl	Hipp CK-p25	Hipp Ctrl	Cerebellum CK-p25	Cerebellum Ctrl
Pithd1	Q8BWR2	PITH domain-containing protein-1	36.9	C188c	HEVTI C# NYESANPADHR	✓					
Adcyap1r1	P70205	Pituitary adenylate cyclase-activating polypeptide type I receptor	80.2	C34c	EQAM C# LER	✓		✓	✓	✓	✓
Atp2b2	Q9R0K7	Plasma membrane calcium-transporting ATPase 2	94.4	C621c	VIEPMA C# DGLR	✓	✓	✓	✓	✓	✓
Atp2b2	Q9R0K7	Plasma membrane calcium-transporting ATPase 2	55.4	C628c	TI C# VAYR					✓	
Plxna4	Q80UG2	Plexin-A4	68.1	C103c	IVQT C# NEPLASTNNVNK	✓					
Pcbp1	P60335	Poly(rC)-binding protein 1	91.9	C194c	VMTIPYQPMPASSPVI C# AGGQDR	✓	✓				
Pcbp1	P60335 Q61990 P57722	Poly(rC)-binding protein 1	60.2	C54c	INISEGN C# PER					✓	✓
Hcn2	O88703	Potassium/sodium hyperpolarization-activated cyclic nucleotide-gated channel 2	55	C69c	DSA C# TPGAAK						✓
Atp12a	Q9Z1W8	Potassium-transporting ATPase alpha 2	91.1	C367c	KN C# LVK				✓	✓	✓
Atp12a	Q9Z1W8 Q8VDN2 Q6PIE5 Q6PIC6 Q9WV27	Potassium-transporting ATPase alpha 2	96.7	C716c	LIIVEG C# QR				✓	✓	✓
Gpr37	Q9QY42	Probable G-protein coupled receptor 37	43.1	C600c	EMSTFASVGTH C#	✓					
Gpr158	Q8C419	Probable G-protein coupled receptor 158	79.8	C1166c	AEV C# PWEFEPLEQPNAER	✓					
Lrp1	Q91ZX7	Prolow-density lipoprotein receptor-related protein 1	70.5	C2518c	ILQEDFT C# R	✓		✓			
Ptges2	Q8BWM0	Prostaglandin E synthase 2	58	C382c	AIEEAPSVHHVNPS C# KD					✓	
Bsn	O88737	Protein bassoon	85.1	C1133c	SS C# SEYSPSPSLDSEAETLDGGPTR	✓					
Fam114a2	Q8VE88	Protein FAM114A2	69.9	C490c	TESST C# EPQSR	✓					
Phf24	Q80TL4	Protein KIAA1045	76.7	C334c	LTEAPS C# SVSISHVGPIADSSPAASSSK	✓					
Prkce	P16054	Protein kinase C epsilon type	68.1	C74c	TNSPAWHDEFVTDV C# NGR	✓					
Prkcg	P63318	Protein kinase C gamma type	90.4	C305c	FEA C# NYPLELYER	✓					
Prkcg	P63318	Protein kinase C gamma type	73.5	C150c	SVPSL C# GVDHTERR	✓				✓	
Prkcg	P63318	Protein kinase C gamma type	60.6	C133c	C# S C# C# EMNVHRR	✓				✓	
Ndrg2	Q9QYG0	Protein NDRG2	82.7	C371c	TLSQSSESGTLPSGPPGHTMEVS C#	✓	✓				
Ndrg3	Q9QYF9	Protein NDRG3	81.1	C375c	HQTMEVS C#	✓	✓	✓	✓		✓
Odr4	Q4PJX1	Protein odr-4 homolog	56.2	C274c C286c	STATVQI C# SGSVNLRGnVK C# R					✓	
Ppp1r1a	Q9ERT9	Protein phosphatase 1 regulatory subunit 1A	72.5	C147c	TQEQ C# GVEPR	✓	✓	✓	✓		
Ppp1r1b	Q60829	Protein phosphatase 1 regulatory subunit 1B	72.9	C148c	GTVGQKPT C# GR	✓	✓	✓	✓	✓	
Ppp1r1b	Q60829	Protein phosphatase 1 regulatory subunit 1B	61.4	C72c	SKRPNP C# AYTPPSLK	✓					

Table S1. SNO-proteins and SNO-Cys sites. SNO-proteins and SNO-Cys sites detected in the cortex, hippocampus and cerebellum of control and CK-p25 mice. The ✔ symbol in the last column indicates the detection of the SNO-peptide using both Approach A and B according to tissue and genotype. SPI %, scored peak intensity obtained with Approach B. Hipp, hippocampus.

Table S1. *SNO*-proteins and *SNO*-Cys sites

Gene Symbol	UniprotKB Access #	Entry name	SPI %	SNO-Site	Sequence (# denotes *SNO*-Cys site)	Cortex CK-p25	Cortex Ctrl	Hipp CK-p25	Hipp Ctrl	Cerebellum CK-p25	Cerebellum Ctrl
Pclo	Q9QYX7	Protein piccolo	71.5	C1222c	VASLA C# EGEQQPDTRPEDLPGATPQTLPKDR	✓					
Shisa9	Q9CZN4	Protein shisa-9	63.9	C397c	LGIAESGS C# DPLGTR	✓					
Dnajc6	Q80TZ3	Putative tyrosine-protein phosphatase auxilin	46.3	C16c	HYQTIQEAGDW C# VPSTEPK	✓					
Rab3gap1	Q80UJ7	Rab3 GTPase-activating protein catalytic subunit	42.2	C919c	SG C# PEER					✓	✓
Rabl6	Q5U3K5	Rab-like protein 6	95.3	C501c	VAPQQ C# SEPETK	✓					✓
Ralbp1	Q62172	RalA-binding protein 1	58.2	C622c	GGIGPPP C# DGVLEVR	✓					
Rap1gap2	Q5SVL6	Rap1 GTPase-activating protein 2	57.1	C565c	TR C# DSASSTPK	✓					
Syngap1	F6SEU4	Ras GTPase-activating protein SynGAP	93.7	C821c	SSPAY C# TSSSDITEPEQK	✓					
Rtn1	Q8K0T0	Reticulon-1	77.4	C64c	EL C# SGPAR	✓	✓	✓	✓	✓	✓
Rtn3	Q9ES97	Reticulon-3	72.9	C559c	V C# SAAPPSVLNETGFSLTVPASAK	✓					
Rtn3	Q9ES97	Reticulon-3	69.7	C344c	TS C# TTESTGLDR	✓	✓	✓	✓		
Rtn4	Q99P72	Reticulon-4	90.6	C319c	SKDKEDLV C# SAALHNPQESPATLTK	✓					
Arhgap5	P97393	Rho GTPase-activating protein 5	58.4	C30c	EPRPPSYTVSVVGLSGTEKDkGN C# GVGk		✓				
Ryr2	E9Q401	Ryanodine receptor 2	38.9	C3008c	EKEMVTSLF C# K	✓					
Atp2a2	O55143	Sarcoplasmic/endoplasmic reticulum calcium ATPase 2	80	C669c	DA C# LNAR	✓	✓	✓	✓	✓	✓
Atp2a2	O55143	Sarcoplasmic/endoplasmic reticulum calcium ATPase 2	83.9	C998c	NYLEQPGKE C# VQPATK	✓				✓	✓
Scrn1	Q9CZC8	Secernin-1	80	C324c	AQSP C# FGDDDPAKKEPR	✓				✓	✓
Sept6	Q9R1T4	Septin-6	65.2	C14c	QVGED C# R	✓					
Sept7	O55131	Septin-7	64.4	C17c	SVN C# GTMAQPK	✓	✓				
Srr	Q9QZX7	Serine racemase	85.5	C217c	VYAAEPSNADD C# YQSK	✓					
Dclk1	Q9JLM8	Serine/threonine-protein kinase DCLK1	79.3	C276c	YQDDFLLDESE C# R	✓					
Dclk2	Q6PGN3	Serine/threonine-protein kinase DCLK2	79	C287c	YAQDDFVLDHSE C# R	✓	✓	✓	✓		
Wnk2	Q3UH66	Serine/threonine-protein kinase WNK2	57	C1946c	AVQTQQP C# SVR	✓					
Tf	Q921I1	Serotransferrin	72.3	C472c	S C# HTGVDR	✓	✓	✓	✓	✓	✓
Tf	Q921I1	Serotransferrin	75.1	C67c	TSYPD C# IK	✓	✓	✓	✓		
Tf	Q921I1	Serotransferrin	84.4	C692c	LLEA C# TFHKH			✓	✓		
Alb	P07724	Serum albumin	76.4	C289c	YM C# ENQATISSK	✓				✓	✓
Sgip1	Q8VD37	SH3-containing GRB2-like protein 3-interacting protein 1	54.9	C402c	E C# GLGQR			✓			
Slc6a11	P31650	Sodium- and chloride-dependent GABA transporter 3	91.7	C607c	TVTVND C# EAK	✓	✓	✓	✓	✓	✓
Atp1a3	Q6PIC6	Sodium/potassium-transporting ATPase subunit alpha-3	76.9	C49c	KYNTD C# VQGLTHSK	✓	✓	✓	✓	✓	✓

Table S1. SNO-proteins and SNO-Cys sites. SNO-proteins and SNO-Cys sites detected in the cortex, hippocampus and cerebellum of control and CK-p25 mice. The ✔ symbol in the last column indicates the detection of the SNO-peptide using both Approach A and B according to tissue and genotype. SPI %, scored peak intensity obtained with Approach B. Hipp, hippocampus.

Table S1. *SNO*-proteins and *SNO*-Cys sites

Gene Symbol	UniprotKB Access #	Entry name	SPI %	SNO-Site	Sequence (# denotes *SNO*-Cys site)	Cortex CK-p25	Cortex Ctrl	Hipp CK-p25	Hipp Ctrl	Cerebellum CK-p25	Cerebellum Ctrl
Atp1a3	Q6PIC6	Sodium/potassium-transporting ATPase subunit alpha-3	90	C221c	SPD C# THDNPLETR	✓	✓	✓	✓	✓	✓
Atp1a3	Q6PIC6	Sodium/potassium-transporting ATPase subunit alpha-3	90.2	C42c	MSVEEV C# RK	✓	✓	✓	✓	✓	✓
Atp1a3	Q6PIC6	Sodium/potassium-transporting ATPase subunit alpha-3	83.5	C49c	YNTD C# VQGLTHSK	✓	✓	✓	✓	✓	✓
Atp1b1	P14094	Sodium/potassium-transporting ATPase subunit beta-1	89.5	C214c	YNPNVLPVQ C# TGK	✓				✓	
Atp1b1	P14094	Sodium/potassium-transporting ATPase subunit beta-1	55.7	C277c	VE C# K	✓	✓	✓	✓	✓	✓
Atp1b2	P14231	Sodium/potassium-transporting ATPase subunit beta-2	68.2	C129c	NDV C# RPGR	✓	✓	✓	✓	✓	✓
Sf1	Q64213	Splicing factor 1	67.7	C279c	SITNTTV C# TK					✓	
Srcin1	Q9QWI6	SRC kinase signaling inhibitor 1	86	C1017c	AIPDLD C# ASK	✓	✓		✓		
Stub1	Q9WUD1	STIP1 homology and U box-containing protein 1	58.2	C200c	AQQA C# IEAK						✓
sygp1	Q8CHC4	Synaptojanin-1	63.8	C1051c	TSP C# QSPTVPEYSAPSLPIRPSRAPSR	✓					
syp	Q62277	Synaptophysin	86.6	C87c	LHQVYFDAPS C# VK	✓	✓	✓	✓	✓	✓
Syp	Q62277	Synaptophysin	73.1	C184c	MATDPENIIKEMPM C# R	✓	✓				
Syp	Q62277	Synaptophysin	61.5	C191c	QTGNT C# K	✓	✓	✓	✓	✓	✓
Syp	Q62277	Synaptophysin	78.9	C184c	EMPM C# R	✓	✓	✓	✓	✓	✓
Snap47	Q8R570	Synaptosomal-associated protein 47	62.4	C330c	G C# TPHRELPTGGQEGEQLQLQK					✓	
Snph	Q80U23	Syntaphilin	62.3	C43c	DAYGTSSLSSSSNSGS C# K	✓					
Stxbp5l	Q5DQR4	Syntaxin-binding protein 5-like	72	C608c	SLSGSTNTVSSEGVTKDSIP C# LSVK	✓					
Tcp1	P11983	T-complex protein 1 subunit alpha	82.2	C357c	I C# DDELILIK	✓					
Tecpr1	Q80VP0	Tectonin beta-propeller repeat-containing protein 1	72.4	C480c	SDE C# RGPASTPAELPWTNIDLKEPK	✓					
Ercc2	O08811	TFIIH basal transcription factor complex helicase XPD subunit	57.3	C134c	C# HSLTASYVR	✓					
Thop1	Q8C1A5	Thimet oligopeptidase	61.2	C687c	GLQVEGSEAPA C#	✓					
Tm2d2	Q8R0I4	TM2 domain-containing protein 2	32.7	C128c	ALEGIE C# AS	✓					
Tceal3	Q8R0A5 Q8CCT4	Transcription elongation factor A protein-like 3	70.3	C142c	E C# ADMTR	✓	✓	✓	✓		✓
Tacc1	Q6Y685	Transforming acidic coiled-coil-containing protein 1	56.6	C479c	KYEAQPLDLDA C# SQDEGAVISK	✓					
Tsn	Q62348	Translin	76	C225c	GFNKETAAA C# GEK					✓	
Tuba1a	P68369 P05213 P68373 P68368	Tubulin alpha-1A chain	78.1	C316c	HGKYMA C# C# LLYRGDVVPK	✓			✓		
Tubb2a	Q7TMM9	Tubulin beta-2A chain	90.7	C354c	TAV C# DIPPR	✓	✓	✓	✓	✓	✓
Tubb2a	Q7TMM9	Tubulin beta-2A chain	79.6	C303c	NMMAA C# DPR	✓	✓	✓	✓	✓	✓

Table S1. SNO-proteins and SNO-Cys sites. SNO-proteins and SNO-Cys sites detected in the cortex, hippocampus and cerebellum of control and CK-p25 mice. The ✔ symbol in the last column indicates the detection of the SNO-peptide using both Approach A and B according to tissue and genotype. SPI %, scored peak intensity obtained with Approach B. Hipp, hippocampus.

Table S1. *SNO*-proteins and *SNO*-Cys sites

Gene Symbol	UniprotKB Access #	Entry name	SPI %	SNO-Site	Sequence (# denotes *SNO*-Cys site)	Cortex CK-p25	Cortex Ctrl	Hipp CK-p25	Hipp Ctrl	Cerebellum CK-p25	Cerebellum Ctrl
Tubb2a	Q7TMM9 Q9CWF2 Q9ERD7 P99024 Q9D6F9 P68372	Tubulin beta-2A chain	79.5	C12c	**MREIVHIQAGQ C# GNQIGAK**	✓	✓	✓	✓	✓	✓
Uchl1	Q9R0P9	Ubiquitin carboxyl-terminal hydrolase isozyme L1	61.6	C152c	**AK C# FEKNEAIQAAHDSVAQEGQ C# R**	✓					
Uba52	P62984	Ubiquitin-60S ribosomal protein L40	71.9	C110c	**AVN C# R**			✓			
Ube2o	Q6ZPJ3	Ubiquitin-conjugating enzyme E2 O	79.1	C593c	**VQS C# PDPAVYGVVQSGDHVGR**	✓					
Uba5	Q8VE47	Ubiquitin-like modifier-activating enzyme 5	71.2	C33c	**SGGDGH C# GR**	✓	✓	✓	✓		✓
Ubxn2b	Q0KL01	UBX domain-containing protein 2B	73.7	C54c	**STPAT C# R**	✓		✓			
Vcam1	P29533	Vascular cell adhesion protein 1	71.3	C668c	**QAQLQDAGIYE C# ESKTEVGSQLR**	✓					
Vcan	Q62059	Versican core protein	86.9	C3258c	**GTVA C# GQPPVVENAK**	✓					✓
Vcan	Q62059	Versican core protein	65.4	C217c	**EG C# YGDMMGK**	✓					
Slc32a1	Slc32a1	Vesicular inhibitory amino acid transporter	26.10	C70c	**SEGEP C# GDEGAEAPVEGDIHYQR**	✓					
Vdac2	Q60930	Voltage-dependent anion-selective channel protein 2	95.1	C48c	**S C# SGVEFSTSGSSNTDTGK**	✓					✓
Cacna2d3	Q9Z1L5	Voltage-dependent calcium channel subunit alpha-2/delta-3	86.8	C969c	**LKQTLEP C# DTEYPAFVSER**	✓					
Cacna1a	P97445	Voltage-dependent P/Q-type calcium channel subunit alpha-1A	71.6	C2327c	**AAG C# ASPR**		✓			✓	
Atp6v1g1	Q9CR51	V-type proton ATPase subunit G 1	71.5	C69c	**EAAALGSHGS C# SSEVEKETR**					✓	
Wfdc1	Q9ESH5	WAP four-disulfide core domain protein 1	65.2	C80c	**C# QADSE C# PR**	✓					

Table S1. SNO-proteins and SNO-Cys sites. SNO-proteins and SNO-Cys sites detected in the cortex, hippocampus and cerebellum of control and CK-p25 mice. The ✔ symbol in the last column indicates the detection of the SNO-peptide using both Approach A and B according to tissue and genotype. SPI %, scored peak intensity obtained with Approach B. Hipp, hippocampus.